JOURNAL OF GEOPHYSICAL RESEARCH, VOL. 98, NO. D11, PAGES 20,369–20,384, NOVEMBER 20, 1993

Experiments Revealing Small Impact of Turbulence on the Energy Budget of the Mesosphere and Lower Thermosphere

F.-J. LÜBKEN, W. HILLERT, G. LEHMACHER, AND U. VON ZAHN

Institute of Physics, Bonn University, Bonn, Germany

We have measured a total of 17 in situ profiles of small-scale density fluctuations (typical resolution: meters) in the lower thermosphere and upper mesosphere, which are used to derive turbulent parameters, such as the turbulent energy dissipation rate ε, the turbulent diffusion coefficient K, and the mean turbulent velocity w_{turb}. The accuracy of the absolute numbers is unprecedented thanks to the very high spatial resolution and a recently improved data analysis procedure. Concentrating on the 12 flights which were performed during winter conditions at high latitudes (69°N), we find mean energy dissipation rates of 1–2 mW kg^{-1} in the lower mesosphere (<75 km) and 10–20 mW kg^{-1} in the upper mesosphere and lower thermosphere (<100 km). The corresponding heating rates are approximately 0.1 and 1 K d^{-1}, respectively. These values are at least 1 order of magnitude smaller than most of the previous measurements and are also significantly smaller than typical values assumed in models. Our observations suggest that the heating effect of turbulence is negligible compared to the most prevailing terms of the heat budget. It can be shown by theoretical considerations involving the turbulent energy budget equation that cooling by turbulent heat conduction is also negligible if ε is small.

1. INTRODUCTION

It is commonly believed that turbulence plays a significant role in the energy budget of the upper atmosphere. Turbulence is a heat source because it transfers potential and kinetic energy from medium scales, for example, generated by the breaking of gravity waves, to very small spatial scales where the energy is converted to heat by viscous dissipation. Typical turbulent energy dissipation rates ε found in the literature for altitudes around the turbopause are 0.1 to 0.5 W kg^{-1} which correspond to heating rates of 8.6 to 43 K d^{-1} [*Justus*, 1967; *Chandra*, 1980; *Gordiets et al.*, 1982; *Ebel et al.*, 1983; *Hocking*, 1990]. If these numbers are correct, turbulent heating is comparable to, or even larger than the other heating mechanisms, such as absorption of solar UV and EUV radiation [*Strobel*, 1978], exothermic chemical reactions [*Nicolet*, 1954; *Mlynczak and Solomon*, 1991*a*], and absorption of terrestrial and tropospheric/stratospheric infrared radiation [*Wehrbein and Leovy*, 1982; *Mlynczak and Solomon*, 1991*b*].

It was realized early that in a stably stratified atmosphere, turbulence also cools the upper mesosphere and lower thermosphere since it transports heat to lower altitudes where it is removed by radiative processes. Unfortunately, it is not clear which effect dominates, heating or cooling. Theoretical studies showed that the net effect of turbulence can be described in terms of a few parameters, for example, the critical flux Richardson number [*Chandra*, 1980; *Zimmerman and Keneshea*, 1986]. These parameters are subject to speculations in the literature since they are very difficult to measure and are therefore only poorly known (in addition, they are expected to vary with altitude and time). Depending on the actual choice of these parameters, some studies arrive at net turbulent heating [*Hunten*, 1974], while others arrive at net cooling [*Johnson*, 1975; *Chandra*, 1980]. Numerical models of the energy budget of the upper atmosphere also give different results [*Gordiets et al.*, 1982; *Ebel et al.*, 1983; *Gärtner and Memmesheimer*, 1984].

The situation is complicated by the fact that turbulence is at least partly created by convective instabilities where the assumption of stable stratification is no longer valid. In general, vertical turbulent motions tend to decrease the potential temperature gradient and thereby reduce the heat conduction of turbulence. Theoretical models of heat fluxes due to convectively unstable gravity waves have shown that turbulence heat fluxes can be reduced dramatically if turbulence is nonuniformly distributed. [*Fritts and Dunkerton*, 1985; *Coy and Fritts*, 1988; *McIntyre*, 1989].

In addition to the direct impact of turbulence on the heat budget described above, turbulence also indirectly affects the thermal structure of the atmosphere, for example, by the transport of photochemically active substances or by the frictional forces on the momentum budget (it is now generally accepted that the breaking of gravity waves induces drag via turbulent friction which changes the global circulation system and finally results in strong heating or cooling, depending on season, due to vertical motions). These indirect influences of turbulence on the heat budget will not be considered in this study.

Considering the importance of turbulence for the upper mesosphere and the uncertainties about its net effect on the energy budget, surprisingly few measurements have been performed in the past (a compilation is presented in the latest version of the COSPAR International Reference Atmosphere, CIRA-1986 *Hocking* [1990]). The main reason for the deficiency of measurements is that turbulence involves very small spatial scales which cannot be resolved by ground-based techniques. Even in situ methods rarely achieve sufficient spatial resolution to measure pure turbulence. The largest contribution to the existing data set stems from composition measurements, from chemical releases, and from radar measurements. The main problem with the latter measurements is that uncertainties are introduced when relating the actual observed quantity (e.g., the radar spectral width) to the geophysically relevant turbulent parameter (e.g., the energy dissipation rate ε). In addition, nonturbu-

Paper number 93JD02055.
0148-0227/93/93JD-02055$05.00

lent processes normally overlay the turbulent signal which may be difficult to account for in the data reduction.

On the basis of our experience with mass spectrometric observations of small-scale density fluctuations in the lower thermosphere [*von Zahn et al.*, 1990], we have developed a relatively simple and cost-effective rocket borne sensor (TOTAL) which allows one to deduce turbulent parameters in the mesosphere and lower thermosphere from very small-scale total density fluctuations. This sensor was flown 17 times in 1990/1991. In this study we will present a summary of these measurements and the implications for the role of turbulence on the heat budget of the upper atmosphere.

2. Turbulent Parameters From Small-Scale Density Fluctuations

Relative Density Fluctuations as a Conservative and Passive Tracer

Turbulence can be measured by its effect on the spatial fluctuations of a conservative and passive tracer. These fluctuations are created by turbulent velocity fluctuations acting on a mean gradient of the tracer. The tracer should be "conservative," which means it should not change in time other than by turbulent motions. In addition, it should be "passive;" that is, it should not influence the turbulent flow.

We use relative neutral density fluctuations as a conservative and passive tracer. These fluctuations are created when an air parcel is moved vertically by turbulent motions. Pressure adjustment between the air parcel and the environment occurs fast since the time constant for turbulent motions is large compared to L/c (L is the typical turbulent length scale, which is equal to 10–100 m; and c is the speed of sound). On the other hand, temperature adjustment occurs slowly because only little heat conduction takes place in the timescale of an turbulent eddy (some minutes). We can therefore assume adiabatic conditions and calculate the density difference between the air parcel and the environment after elevation by Δz. The relative difference is given by [*Thrane and Grandal*, 1981; *Lübken*, 1992]

$$\frac{\Delta n}{n} \approx \left(\frac{1}{H_n} - \frac{1}{\gamma H_p}\right)\Delta z = \frac{\omega_B^2}{g}\,\Delta z \qquad (1)$$

where

Δn density difference between the air parcel and the environment;

n mean density;

H_n, H_p scaleheights for density and pressure;

$\gamma = c_p/c_v$ ratio of specific heats;

$\omega_B = [(g/T)(\partial T/\partial z + \Gamma)]^{1/2}$ Brunt-Väisälä frequency;

$\Gamma = -g/c_p$ adiabatic lapse rate of temperature;

$\partial T/\partial z$ vertical component of the temperature gradient (throughout the paper we assume that horizontal temperature gradients are small compared to vertical).

These relative density fluctuations are indeed a conservative tracer since they are conserved in adiabatic motions. In addition, this tracer certainly meets the requirement of passiveness, since typical turbulent density fluctuations are of the order of 0.1–1% (see below), which is too small to significantly influence the turbulent flow.

Turbulent Parameters From a Spectral Model

The main aim of our data reduction is to deduce geophysically relevant parameters, as for example the turbulent energy dissipation rate ε, from the measured density fluctuations. As is described in more detail by *Lübken* [1992], we have used the "spectral model method" since it avoids uncertainties and ambiguities which are present in other methods. We fit a theoretical spectral model to the measured turbulent spectrum by adjusting two free parameters. The geophysically relevant quantities are then obtained from these parameters. It turns out that the "inner scale," that is, where the inertial and the viscous subrange of the spectrum merge, basically determines the value obtained for the energy dissipation rate. We have applied a model first presented by *Heisenberg* [1948], which exhibits the classical $k^{-5/3}$ power law in the inertial subrange and the k^{-7} behavior in the viscous subrange. Between these subranges a smooth transition takes place. The frequency spectrum is given by

$$W(\omega) = \left[\frac{\Gamma(5/3)\,\sin\,(\pi/3)}{2\pi v_R}\right] C_n^2 f_\alpha \left[\frac{(\omega/v_R)^{-5/3}}{[1 + \{(\omega/v_R)/k_0\}^{8/3}]^2}\right] \qquad (2)$$

where Γ is the Gamma function ($\Gamma(5/3) = 0.90167$, (which should not be mixed with the adiabatic lapse rate), v_R is the rocket velocity, $C_n^2 = a^2 N_n/\varepsilon^{1/3}$ is the structure function constant; ε is the dissipation rate of energy, and N_n represents the amount of inhomogeneity which disappears per unit time due to molecular diffusion. We will call the latter quantity "inhomogeneity dissipation rate" throughout this paper. The factor f_α (= 1 or 2) takes into account the different normalizations used for N_n (see *Lübken* [1992] for more details). The numerical constant a^2 is determined from experiments. It is related to the Obukhov-Corrsin constant β and to another constant A used later:

$$\beta = \frac{\Gamma(8/3)}{\pi}\,a^2\,\sin\,(\pi/3) = 0.414a^2 = 4\pi A; \qquad A = 0.033a^2 \qquad (3)$$

where $\Gamma(8/3) = (5/3)\Gamma(5/3) = 1.5028$. Following the recommendation of *Hill* [1978], we use $\beta = 0.72$; thus $a^2 = 1.74$ and $f_\alpha = 2$. The normalization of the frequency spectrum in (2) is such that $\sigma^2 = \int_{-\infty}^{\infty} W(\omega)\,d\omega$, where σ is the variance of the fluctuations. The Heisenberg model "breaks" at a wavenumber $k_0 \equiv \omega_0/v_R$, which is the intersection of the asymptotic forms of $W(\omega)$ in the inertial and viscous subrange, respectively. As is explained by *Lübken and Hillert* [1992], k_0 is determined by the behavior of the structure function at the origin, which imposes a constraint on $W(\omega)$. The final result for the breakpoint scale (also called the inner scale) $l_0^H \equiv (2\pi)/k_0$ is

$$l_0^H/\eta = 2\pi\left\{\frac{9f_\alpha a^2\Gamma(5/3)\sin(\pi/3)}{16Pr_n^{\mathrm{mol}}}\right\}^{3/4} = 9.90; \qquad \eta = \left(\frac{\nu^3}{\varepsilon}\right)^{1/4} \tag{4}$$

where $Pr_n^{\mathrm{mol}} = 0.83$ is the molecular Prandtl number [*Chapman and Cowling*, 1970]. The parameter η is called the Kolmogoroff microscale.

We have tentatively used a second model in our data reduction which is presented by *Tatarskii* [1971] and which goes back to *Novikov* [1961]. It also consists of the classical inertial subrange behavior but exhibits an exponential drop-off for wavenumbers larger than k_m. The three-dimensional power spectrum in the wavenumber space is given by

$$\Phi(k) = \frac{AN}{\varepsilon^{1/3}}k^{-11/3}\exp(-k^2/k_m^2) = \frac{5}{12\pi^2}\Gamma(5/3)\sin(\pi/3)C_n^2 k^{-11/3}\exp(-k^2/k_m^2) \tag{5}$$

The corresponding frequency spectrum is obtained from $W(\omega) = (2\pi/v_R)\int_{|\omega|/v_R}^{\infty}\Phi_\vartheta(k)k\,dk$. It is proportional to an incomplete gamma function which is calculated using computer library programs. Again, the constraint imposed by the behavior of the structure function at the origin determines k_m and the corresponding inner scale $l_0^T \equiv (2\pi)/k_m$:

$$l_0^T/\eta = 2\pi\left\{\frac{3f_\alpha a^2(5/3)\Gamma(5/3)^2\sin(\pi/3)}{4\pi Pr_n^{\mathrm{mol}}}\right\}^{3/4} = 7.06 \tag{6}$$

As will be shown later, the energy dissipation rates determined from the spectrum are "not" sensitive to the particular model used (Heisenberg or Tatarskii). We have adopted Heisenberg's model in our standard data analysis since it is somewhat easier to evaluate than Tatarskii's model. Once the inner scale l_0^H (or alternatively l_0^T), the energy dissipation rate ε, and the inhomogeneity dissipation rate N_n are determined, further turbulent parameters of interest are derived, such as the turbulent diffusion coefficient for momentum K_m, the mean turbulent velocity w_{turb}, and the outer scale L_B [*Weinstock*, 1978*a*; *Weinstock*, 1981]:

$$K_m = Ri\frac{\varepsilon}{\omega_B^2} = \varepsilon\Big/\left(\frac{\partial u}{\partial z}\right)^2 \tag{7}$$

$$w_{\mathrm{turb}} = [(\varepsilon/0.49\omega_B)]^{1/2} \tag{8}$$

$$L_B = 9.97\,[(\varepsilon/\omega_B^3)]^{1/2} \tag{9}$$

where Ri is the gradient Richardson number defined by $Ri = \omega_B^2/(\partial u/\partial z)^2$, and u is the horizontal wind.

It should be noted that the models introduced above assume that the fluctuations are homogeneous, isotropic, and stationary. These are very strong conditions which seem to be rather unlikely in the real atmosphere. For example, one would not expect isotropic conditions at scales, where buoyancy forces are more important than inertial forces or viscous forces. However, our main result relies on very small scales of a few meters only, where buoyancy forces can be neglected compared to the other forces and anisotropy may be less important. The satisfactory agreement between the measured spectra and the turbulent models presented later supports this view. However, we cannot positively exclude the influence of nonisotropy and nonstationarity, and this should be kept in mind when regarding the errors presented later.

Weinstock's relations cited above were derived for stratified homogenous turbulence and should therefore also be used with some care. However, they are frequently used in the literature to obtain K from ε and have therefore also been used in our data reduction in order to facilitate comparison with data obtained by other methods.

Role of the Background Atmosphere

A reliable measurement of the background atmosphere, especially density and temperature, should always accompany measurements of turbulence for several reasons. For example, the ε values deduced from l_0^H (or from l_0^T) depend on the kinematic viscosity, thus on density and temperature:

$$\nu = \mu/\rho; \quad \mu = \frac{\beta T^{3/2}}{T+S} \tag{10}$$

where μ is the dynamic viscosity, β is a constant equal to 1.458×10^{-6} kg/(s m $K^{1/2}$) and S is Sutherland's constant, equal to 110.4 K. Furthermore, the conversion of turbulent velocity fluctuations to variations of the passive tracer depends on the background gradient of the tracer, which in our case depends on the temperature profile. We have noted earlier that the gradient of the relative density fluctuations is given by ω_B^2/g (see equation (1)). Therefore the "sensitivity" of neutral density fluctuations as a passive tracer for turbulence depends on ω_B^2: the larger the difference between the actual temperature gradient (more precisely: the vertical component of it) and the adiabatic lapse rate, the more sensitive is this method. In the case of $\omega_B = 0$ (atmospheric temperature profile exhibits adiabatic lapse rate), no fluctuations will be created, even if strong turbulence is present: our technique is "blind" to detect turbulence in this case. This is evident from another point of view: in an atmosphere with an adiabatic lapse rate a vertical excursion of an air parcel will not create any density fluctuations because the excursion is an adiabatic process, at least in good approximation.

Could it be that our mean ε values (presented later) are systematically biased toward too low values because the atmosphere is frequently in a status of zero potential temperature gradient? There are a number of experimental facts which indicate that this is not the case; as will be explained later, we have measured temperature profiles nearly simultaneously with the TOTAL flights by (1) TOTAL itself (above 90 km), (2) falling spheres (90–35 km), and (3) various lidars. We have performed a statistical analysis for all 14 winter flights and have found that in the altitude range of 60–100 km, only in approximately 5% of all altitude bins of 1 km width is the temperature lapse rate less than or equal to the adiabatic lapse rate (the error bars of the measured temperatures have been considered in these statistics). No systematic altitude dependence was observed. Therefore our results are most likely not severely influenced by the "blindness" effect mentioned above. It should be pointed out that

the location of the inner scale, and thus the derived energy dissipation rate, does not depend on ω_B. In other words, as long as the "sensitivity" is large enough that TOTAL can see the break in the spectrum, the ε values obtained are independent of ω_B. Further support that our values are not biased stems from the intercomparison between TOTAL and PIP (positive ion probe) which was mounted on the same payload as TOTAL [*Lübken et al.*, 1993*a*]. Ion fluctuations are not sensitive to adiabatic lapse rates due to different scale heights of neutrals and ions. The good agreement found in the range of overlapping data (65–90 km) confirms the low energy dissipation rates observed by TOTAL.

Apart from the direct need for background parameters discussed above, they can also help to identify possible sources of turbulence. The temperature measurements mentioned above have been combined with high-resolution measurements of the chaff technique in the altitude range 80–90 km [*Widdel*, 1987] to calculate Richardson numbers, which, if below a critical value, indicate unstable conditions. A detailed analysis on possible sources for turbulence has been presented for the flights of the DYANA campaign in *Lübken et al.* [1993*a*]. Most turbulent layers were indeed associated with small Richardson numbers. We will not discuss this aspect of our measurements any further in this study.

Typical Length Scales for Turbulence

Typical length scales for the inner and outer scale (l_0^H and L_B) expected in the mesosphere are shown in Figure 1 as a function of altitude. For comparison reasons we also show the Kolmogoroff microscale η, and the mean free path λ, taken from CIRA-1986 [*Fleming et al.*, 1990]. The profiles in Figure 1 are calculated for an energy dissipation rate of ε = 100 mW kg^{-1}. This is considered a typical order of magnitude value in the literature, but it is too large according to our measurements presented later. However, according to equation (4), the inner scale l_0^H and the Kolmogoroff microscale η would only be a factor of $10^{1/4} = 1.78$ larger if we had chosen 10 mW kg^{-1} for ε (at the same time L_B would decrease by a factor of $10^{1/2} = 3.16$ which would limit the inertial subrange to altitudes below approximately 100 km).

As expected, the smallest turbulent scales of size η are much larger than the mean free path λ. The inertial subrange (hatched area in Figure 1) diminishes with increasing altitude and disappears above ~110 km because of increasing kinematic viscosity. In order to detect the inner scale l_0^H in the whole mesosphere, the spatial resolution of the instrument has to be of the order of 1–10 m. For a rocket-borne sensor with a typical velocity of 1000 m s^{-1}, this corresponds to a time constant of 1–10 ms.

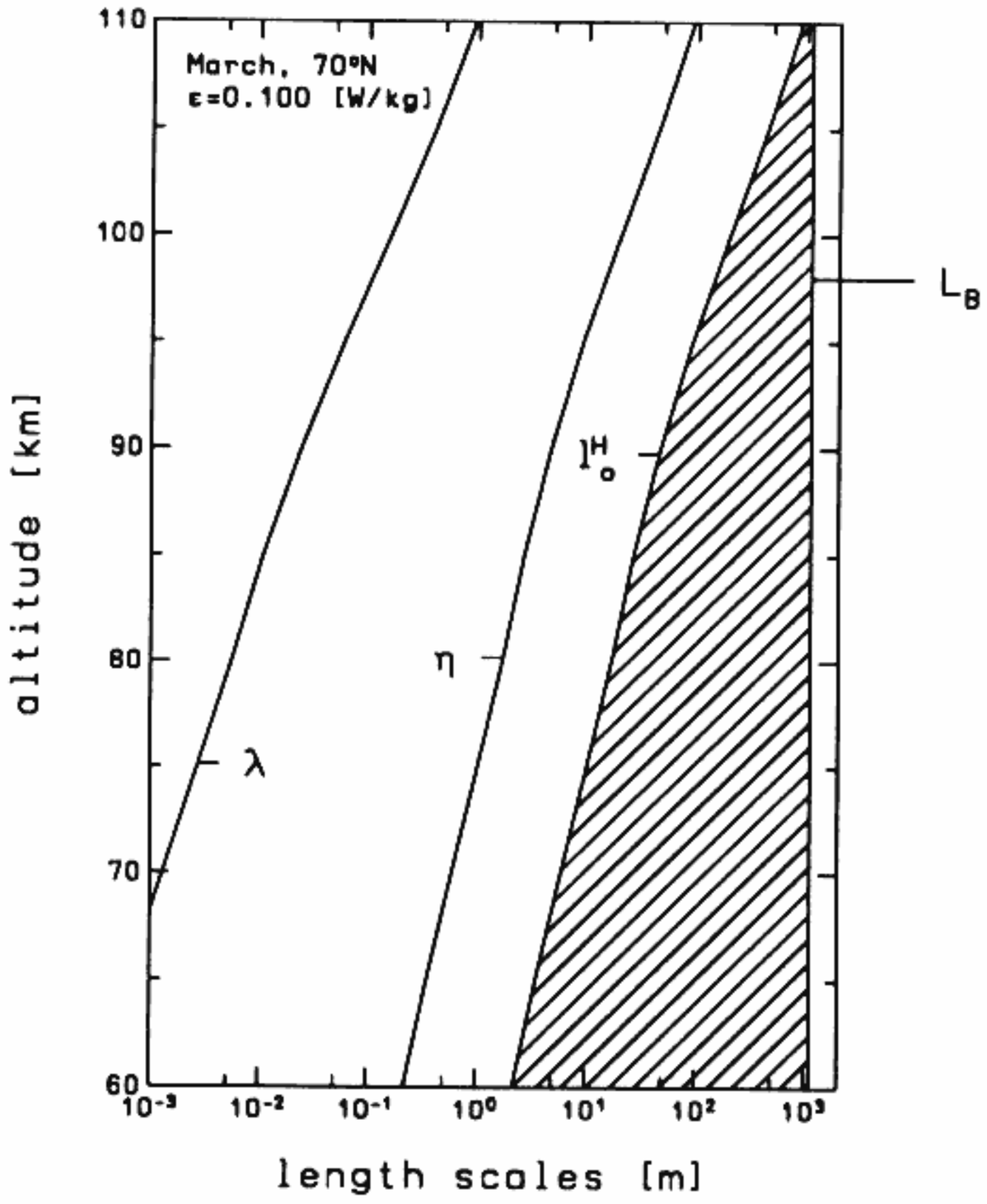

Fig. 1. Length scales of importance for turbulence: L_B, outer scale; l_0^H, inner scale (definition from Heisenberg spectrum); η, Kolmogoroff microscale; and λ, mean free path (for definitions and explanations, see text). A constant energy dissipation rate of ε = 100 mW kg^{-1} is assumed at all altitudes. The atmospheric background parameters such as the Brunt-Väisälä frequency ω_B and kinematic viscosity ν are taken from CIRA-1986 (March, 70°N). The inertial subrange is shown hatched.

3. EXPERIMENTAL METHOD

TOTAL Instrument on Board the TURBO Payload

The name TOTAL indicates that this instrument measures total gas densities rather than a particular constituent (like a mass spectrometer). Only a brief description is given here emphasizing the most important instrumental parameters. Technical details of the TOTAL instrument and the TURBO payload have been presented in the literature [*Hillert et al.*, 1993]. The TOTAL instrument basically consists of an ionization gauge which is mounted in the rear of the payload. The most important instrumental parameter is the time constant: the number density inside the sensor follows a sudden increase of ambient density only with a certain time constant, τ_s. This time constant has been measured in the laboratory for a wide range of pressures. The result is $\tau_s \sim$ 8 ms^{-} for $p < 2 \times 10^{-3}$ mbar and ~ 1–3 ms for $p > 10^{-2}$ mbar [*Hillert et al.*, 1993]. These numbers include the time constant of the electronics (~0.5 ms). The dependence of τ_s on pressure is favorable for our application because at higher altitudes (corresponding to smaller pressures) the size of the smallest eddies increases due to the increasing kinematic viscosity (see Figure 1). This results in larger time periods of the density fluctuations caused by these eddies. In Figure 2 we compare τ_s with the time constant required to resolve spatial scales of the order of l_0^H for various ε values. As can be seen from this figure, the sensor time constant is sufficiently small to detect the inner scale in the whole altitude range of interest, even for very large energy dissipation rates of 1000 mW kg^{-1} (which were never observed by TOTAL).

As is described in more detail by *Hillert et al.* [1993], other important instrumental parameters of TOTAL are high sensitivity (typical ion currents of 2, 13, and 830 nA at 110, 90, and 70 km, respectively), a wide range of pressures (10^{-5} to 1 mbar), fast and reliable electronics and telemetry (4880 samples s^{-1}, 12-bit resolution), and low instrumental noise (0.02–0.1% of the signal).

The TOTAL instrument measures atmospheric neutral gas

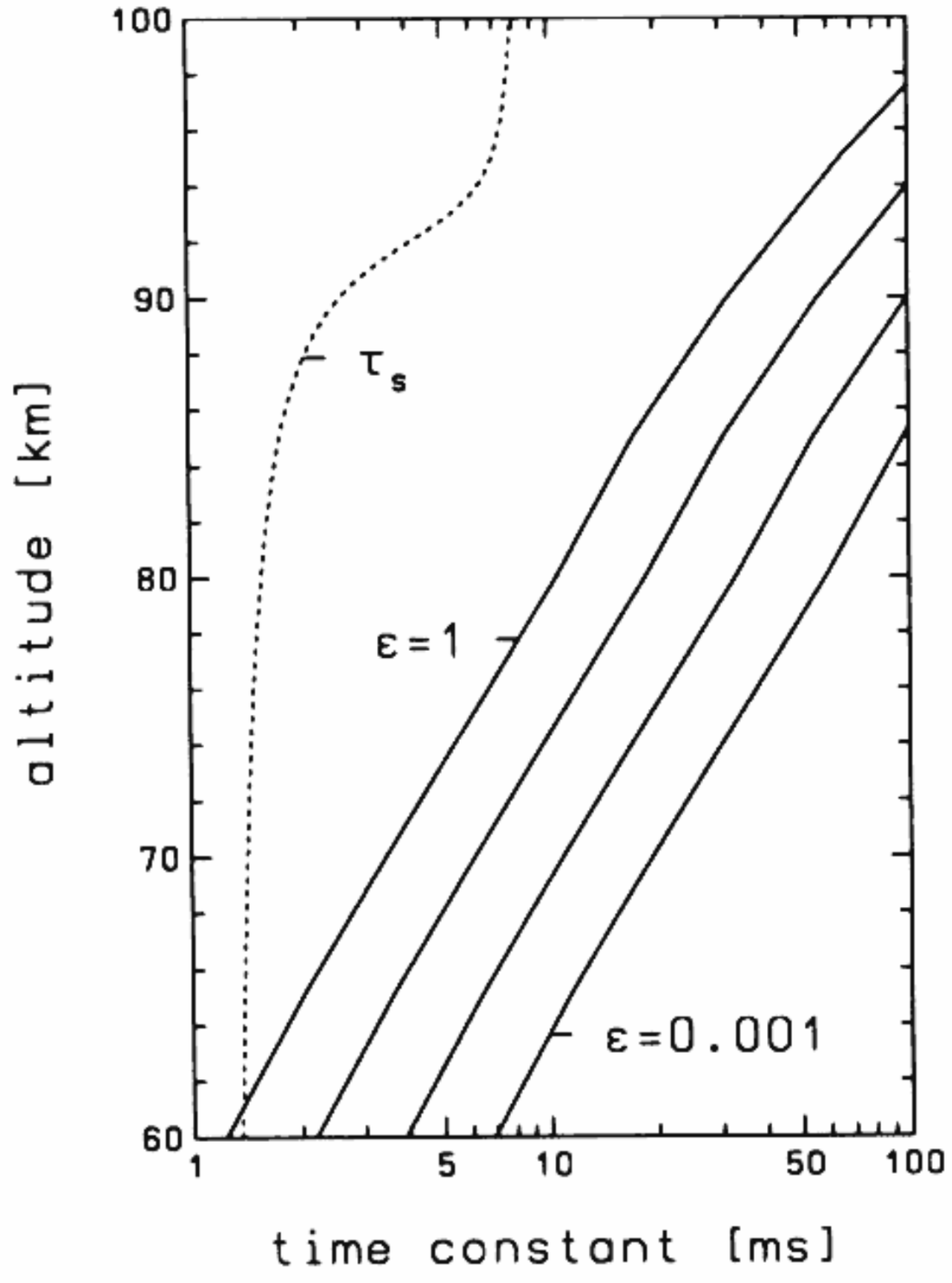

Fig. 2. Time constant of the TOTAL sensor τ_s as a function of altitude. The parameter τ_s has been measured in the laboratory for various pressures [*Hillert et al.*, 1993]. Pressures typically measured inside the sensor during flight have been used to calculate the τ_s profile. For comparison, the time constants needed to resolve the inner scales l_0^H (the smallest scales of the inertial subrange) are shown for various strength of turbulence, that is, for various energy dissipation rates ε (in watts per kilogram). The definition of inner scale according to Heisenberg's spectral model has been used. Kinematic viscosities needed to calculate these time constants were taken from CIRA-1986 for March and 70°N.

density fluctuations from apogee (≈130 km) to approximately 65 km. Absolute atmospheric number densities are measured from 115 to 90 km only. The reason for this more limited region is the unknown effect of atomic oxygen on the number densities inside the sensor above ~115 km and the correction of the aerodynamic pressure enhancement below ~90 km: since the sensor moves through the atmosphere, the density inside the sensor is significantly increased compared to ambient number density. This enhancement is corrected for in the data reduction, however, only at altitudes where molecular flow conditions are present (approximately above 90 km). Atmospheric temperatures are deduced from absolute densities assuming hydrostatic equilibrium. The procedure to obtain ambient number densities and temperatures is described elsewhere [e.g., *Friker and Lübken*, 1992].

TURBO Payload and the Rocket Flights

The TURBO payload was especially designed and built for high-resolution neutral and plasma turbulence measurements. It reaches an apogee of typically 130 km after 3 min of flight and impacts in the ocean (on land for the two flights from Esrange) at a range of 80–100 km, 11 min after launch. The TOTAL measurements take place on the downleg part of the flight from apogee to ~65 km. In order to perform a reasonable number of measurements it was necessary to make the TURBO flights cost effective. This was possible thanks to the sea recovery capability of the payload. A total of 17 flights were performed with TURBO in 1990–1991. The payload was recovered 13 times (11 successful sea recoveries and two land recoveries) which is excellent considering that the sea recovery technique was newly developed by the DLR (Deutsche Forschunganstalt für Luftund Raumfahrt) in Oberpfaffenhofen, Germany. The instruments performed successfully in all flights.

Apart from TOTAL there are two more instruments on the TURBO payload which are property of the Norwegian Defence Research Establishment (NDRE): a probe mounted around TOTAL which measures the fluctuations of positive ion number density on downleg (PIP), and a second probe in the front of the payload which measures positive ions on upleg and electrons on downleg (EPIP) [*Blix et al.*, 1993]. We will later compare our TOTAL results with the turbulent parameters obtained from the ion fluctuation measurements (electrons are less suitable since they are influenced by instrumental effects).

Supporting Measurements by Falling Spheres, Foil Clouds, and Lidars

For the reasons discussed above, the TURBO flights were normally accompanied by so-called "meteorological rockets" which determine densities, temperatures, and wind (not used in this study). Furthermore, lidar measurements of densities and temperatures were also performed simultaneously, whenever weather conditions and operational constraints permitted. The above mentioned techniques will not be described here since they have been extensively presented in the literature (some references of particular interest are listed below). The derived quantities and the altitude ranges of the measurements are (1) falling sphere: densities, temperatures and winds from ~95 (temperatures: 90) to 35 km [*Jones and Peterson*, 1968; *Schmidlin*, 1991], (2) sodium lidar: temperatures from 85 to 105 km [*Fricke and von Zahn*, 1985; *Neuber et al.*, 1988], and (3) Rayleigh lidar: densities and temperatures from 35 to 85 km [*Hauchecorne and Chanin*, 1980; *Czechowsky et al.*, 1991].

Only the sodium lidar measures temperatures directly; the others measure primarily density, and the temperature profile is obtained by (downward) integration of the density profile assuming hydrostatic equilibrium.

Flights and Campaigns

The TURBO payload was flown 17 times in the following three campaigns: Dynamics Adapted Network for the Atmosphere (DYANA) in early 1990, noctilucent cloud in August 1991 (NLC-91) and METAL (metal layers were studied) in August/September 1991. A list of all rocket flights during the various campaigns is presented in Table 1. More details about the scientific objectives of these campaigns, the instruments employed, and the launch dates of all rocket flights (including meteorological rockets) can be found elsewhere [*Offermann*, 1991; *Goldberg et al.*, 1993; also U. von Zahn, manuscript in preparation, 1993]. Most of the TURBO flights were performed at high latitudes: 12 from Andøya

TABLE 1. Launch Dates of the TURBO Payload Equipped With the TOTAL Instrument

Label	Date	Time, UT
	DYANA in Andøya (69°N)	
DAT13	Jan. 22, 1990	1115:00
DAT50	Feb. 25, 1990	1920:00
DAT62	March 6, 1990	0241:00
DAT73	March 8, 1990	2253:00
DAT76	March 9, 1990	0025:00
DAT84	March 11, 1990	2042:00
	DYANA in Biscarosse (44°N)	
DBN 1	Feb. 20, 1990	0454:00
DBN 2	March 6, 1990	0518:28
DBN 3	March 13, 1990	0421:00
	NLC-91 in Kiruna (68°N)	
N-3T05	Aug. 1, 1991	0140:00
N-AT13	Aug. 8, 1991	2315:00
	METAL in Andøya (69°N)	
LT1	Sept. 17, 1991	2343:00
LT6	Sept. 20, 1991	2048:00
LI9	Sept. 20, 1991	2240:00
LT13	Sept. 30, 1991	2055:15
LT17	Oct. 3, 1991	2227:30
LT21	Oct. 4, 1991	0008:00

A complete list of all rocket launches in the various campaigns, including the meteorological rockets of interest can be found in the summary articles of the campaigns.

(69°N, 16°E) and 2 from Kiruna (68°N, 21°E). Three TURBOs were launched from Biscarosse (Centre d'Essais des Landes; 44°N, 1°W) in Southern France.

4. RESULTS

Residuals and Spectra

In Figure 3, two extracts of residuals obtained during rocket flight LT06 of the METAL campaign are shown. In the upper panel, strong small- and medium-scale fluctuations are observed. In order to demonstrate that these fluctuations are due to atmospheric density fluctuations and are not an instrumental artifact, we show another extract from the same flight, just 4 km higher (lower panel of Figure 3). Comparison between the two altitude bins clearly shows that there is a region around 79 km with strong atmospheric fluctuations presumably caused by turbulence, whereas no fluctuations are observed around 85 km (the small remaining fluctuations of <0.1% are due to instrumental noise). This is typical for our measurements: regions with enhanced turbulent activity alternate with very quiet regions.

In Figures 4 and 5 the power spectral densities $|c_k|^2$ of the percentage fluctuations in Figure 3 are shown as a function of frequency f. We have used subroutine RFFT from the CERN computer library, where the normalization of the Fourier coefficients c_k is such that

$$2 \sum_{k=0}^{N/2} |c_k|^2 = \sigma^2 \tag{11}$$

and the frequencies are given by

$$f_k = \frac{k}{2N\Delta t} \tag{12}$$

(N is the number of residuals, all equidistant in time with time difference Δt; σ is the variance). In order to use the same normalization for the theoretical spectra we transform $W(\omega)$ to

$$\text{PSD}\ (f_k) = W(\omega_k)\Delta\omega \times 10^4 = W(2\pi f_k)2\pi\Delta f \times 10^4$$

$$\Delta f = \frac{1}{2N\ \Delta t}$$

and compare PSD (f_k) with the experimental spectrum in Figures 4 and 5 (factor 10^4 because of percentage fluctuations).

We have fitted the Heisenberg model of (2) to the spectrum in Figure 4. From the best fit model we get the energy dissipation rate ε and the inhomogeneity dissipation rate N_n. From this we calculate the other turbulent parameters listed above, where we have used the density and temperature profiles from TOTAL and from the falling sphere. The results are summarized in Table 2.

As can be seen from Figure 4, the Heisenberg spectrum nicely fits the measured spectrum. The energy dissipation rate determined from the best fit is 13.8 ± 4 mW kg^{-1}. The inner and outer scale are l_0^H = 24.9 m and L_B = 359 m, respectively. This means that the inertial subrange extends over more than 1 order of magnitude. The best fit result obtained for N_n is 2.05×10^{-7} s^{-1} with an error of 20%. In Figure 4 we have also plotted the Tatarskii model using the above values obtained from the Heisenberg model. Tatarskii's model also nicely fits the observed spectrum, although the fit parameters are not optimized for this model. In fact, the two models can hardly be distinguished in Figure 4. This suggests already that the results are not very sensitive to the specific model used. To investigate this subject further, we have independently fitted Tatarskii's model to the spectrum in Figure 4. The result is ε = 12.0 ± 3 mW kg^{-1} and N_n = 1.99 ± 10^{-7} s^{-1}. Both values are in good agreement with the results obtained from the Heisenberg model fit. We therefore arrive at the important conclusion that the results of the model fit are not very sensitive to the specific model used, at least within acceptable accuracy limits.

The power spectrum of the residuals in the quiet layer of Figure 3 is shown in Figure 5. What was obvious from the residuals already is also clear from the spectrum: there is no turbulence present in this altitude bin. The spectrum basically consists of instrumental noise. To demonstrate the sensitivity of our instrument, we have plotted the theoretical spectra of Heisenberg and Tatarskii that we would expect if there were any significant turbulence present. We have assumed energy dissipation rates of 1, 10, and 100 mW kg^{-1} and the inhomogeneity dissipation rate N_n from the upper panel in Figure 3. Since the theoretical spectra in the inertial subrange are proportional to $C_n^2 = a^2 N_n/\varepsilon^{1/3}$, an increase (decrease) of ε and N_n by a factor of 10 leads to an upward (downward) shift of the spectrum by a factor of $10^{2/3} = 4.6$. It is obvious from Figure 5 that the measured spectrum is not compatible with turbulence, even for very low energy dissipation rates. Furthermore, this figure demonstrates that the sensitivity of our instrument to measure ε is certainly better than 1 mW kg^{-1}. It should be mentioned, however, that this sensitivity also depends on N_n: if N_n is smaller by a certain factor than assumed in Figure 5, the theoretical spectra are shifted downward by this factor. This can limit the sensitivity if ω_B^2 is very small (remember that $N_n \propto \omega_B^2$).

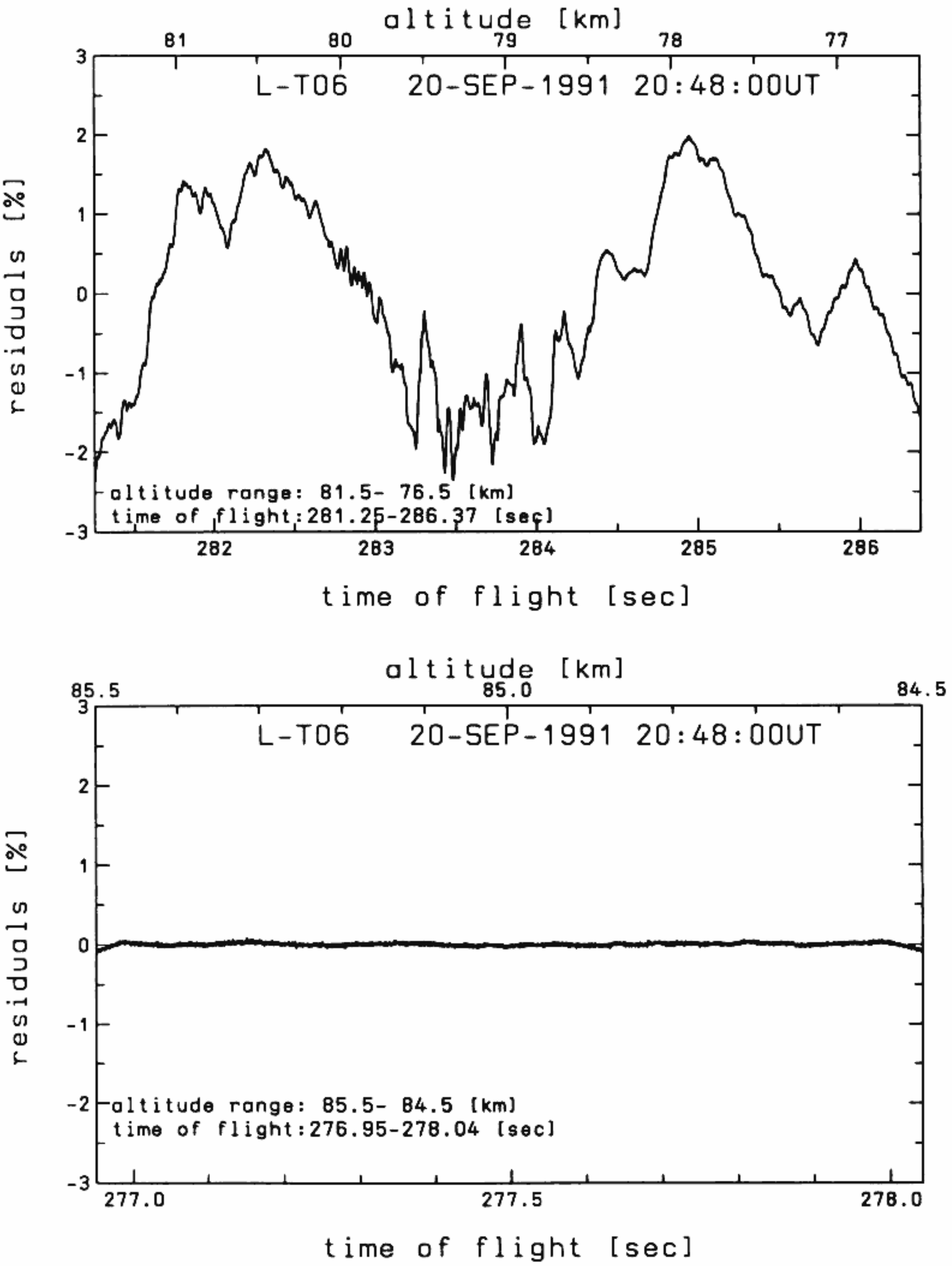

Fig. 3. Relative density fluctuations (residuals) for METAL flight LT6. (top) From 81.5–76.5 km (time of flight: 281.25–286.37 s). Strong fluctuations presumably caused by turbulent motions are present in this altitude bin. (bottom) From 85.5–84.5 km (time of flight: 276.95–278.04 s). No density fluctuations are observed in this altitude regime. The remaining small fluctuations of <0.1% are due to instrumental noise.

Summary of TOTAL Measurements

In Figure 6 all energy dissipation rates measured by TOTAL during the DYANA campaign are shown together with the running mean over 5 km (we also show the expected lower limit $\varepsilon_{min} = \nu\omega_B^2$, derived from theory). Typical energy dissipation rates are around 1 mW kg^{-1} below ~75 km, increasing to ~20 mW kg^{-1} in the upper mesosphere. The corresponding heating rates are of the order of 0.1 and 2 K d^{-1}, respectively. The minimum/maximum ratio of the data in a given altitude bin is approximately 20 with no distinct height structure. This is in line with the observations of temperature profiles in winter which suggest that there is approximately the same variability in the whole mesosphere.

In Figure 7 the mean ε profiles obtained during the three campaigns at high latitudes are summarized (only the three flights from Biscarosse are not presented in this plot). Although performed in late winter and in autumn, respectively, we will regard both the DYANA and the METAL results as typical for the winter season. This is justified if we consider the seasonal behavior of the dynamical and thermal structure in the mesosphere [e.g., *Lübken and von Zahn*, 1991].

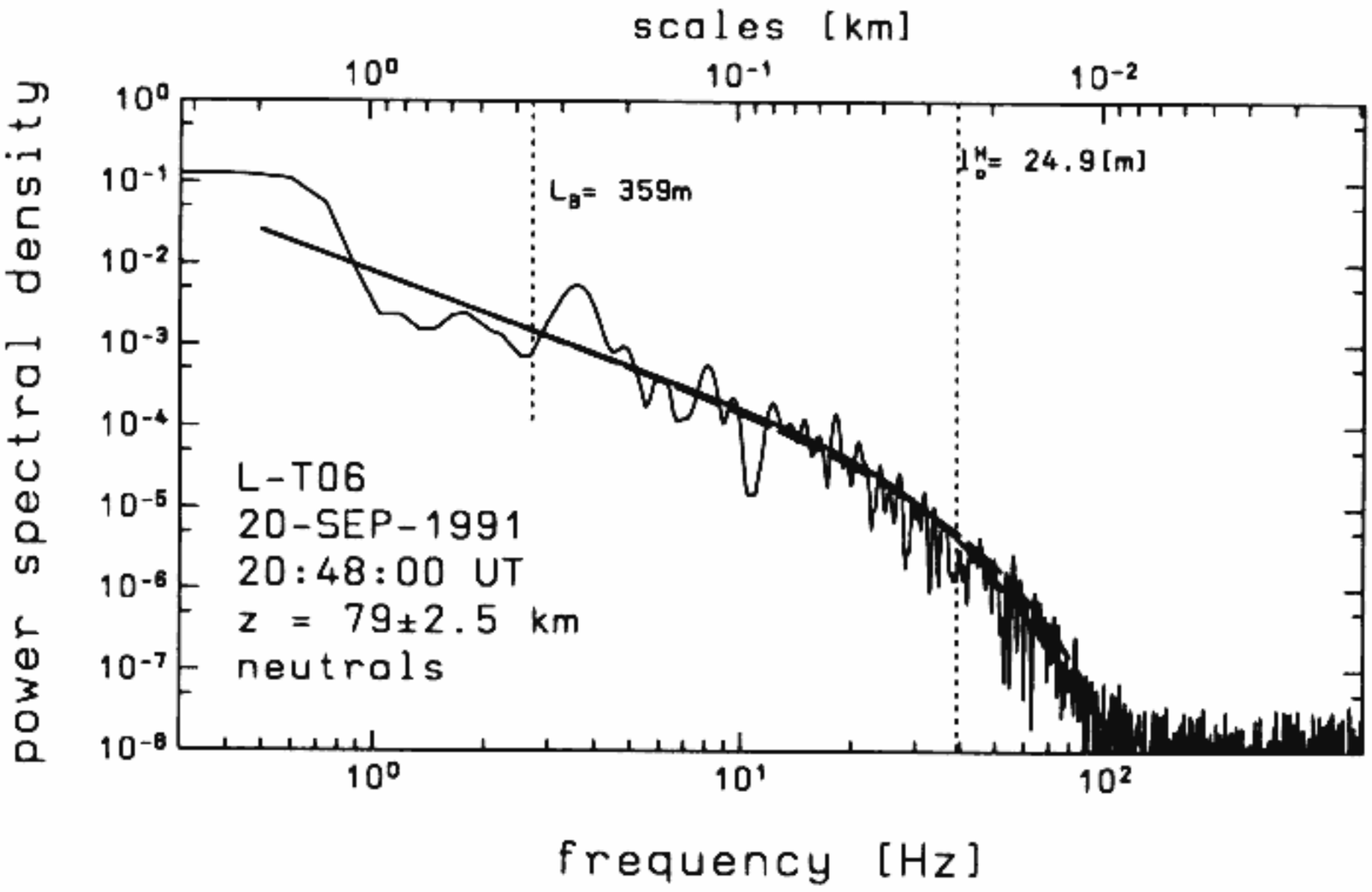

Fig. 4. Power spectrum of the residuals of Figure 3 (upper panel), together with Heisenberg's (solid line) and Tatarskii's (dashed line) theoretical model (the two models are almost identical). The best fit value for the energy dissipation rate as determined from the Heisenberg model is 13.8 mW kg^{-1}. The other parameters are listed in Table 2. For normalization of the spectrum, see text. The Heisenberg inner scale l_0^H and the outer scale L_B are also shown. The upper scale shows the spatial scales derived from $L \equiv \lambda = 2\pi/k = v_R/f$ (f = frequency; v_R = rocket velocity = 977 m s^{-1}).

A comparison between the DYANA and the METAL mean profile in Figure 7 shows that the low-energy dissipation rates obtained during DYANA were not unique: during METAL we again observe very small ε values. In fact, in the upper mesosphere the mean profile during METAL is even smaller than during DYANA, although only by a factor of 5 which is within the natural variability. Both the DYANA and the METAL data suggest that the mean energy dissipation rate in the lower mesosphere is very low (1–2 mW kg^{-1}) and increases to moderate values (~10–20 mW kg^{-1}) in the upper mesosphere. As we will see later, these numbers are significantly smaller than what is considered typical for these altitudes. Throughout the whole mesosphere mean heating rates are below 2–3 K d^{-1}, which is small compared to the competing heating and cooling processes in the upper mesosphere. We have calculated a total mean profile of all winter data (DYANA + METAL) which was further smoothed by a 5-point running mean. This profile is shown as a thick solid line in Figure 7 and will later be used for intercomparison with other measurements and models. The numbers are listed in Table 3 for reference.

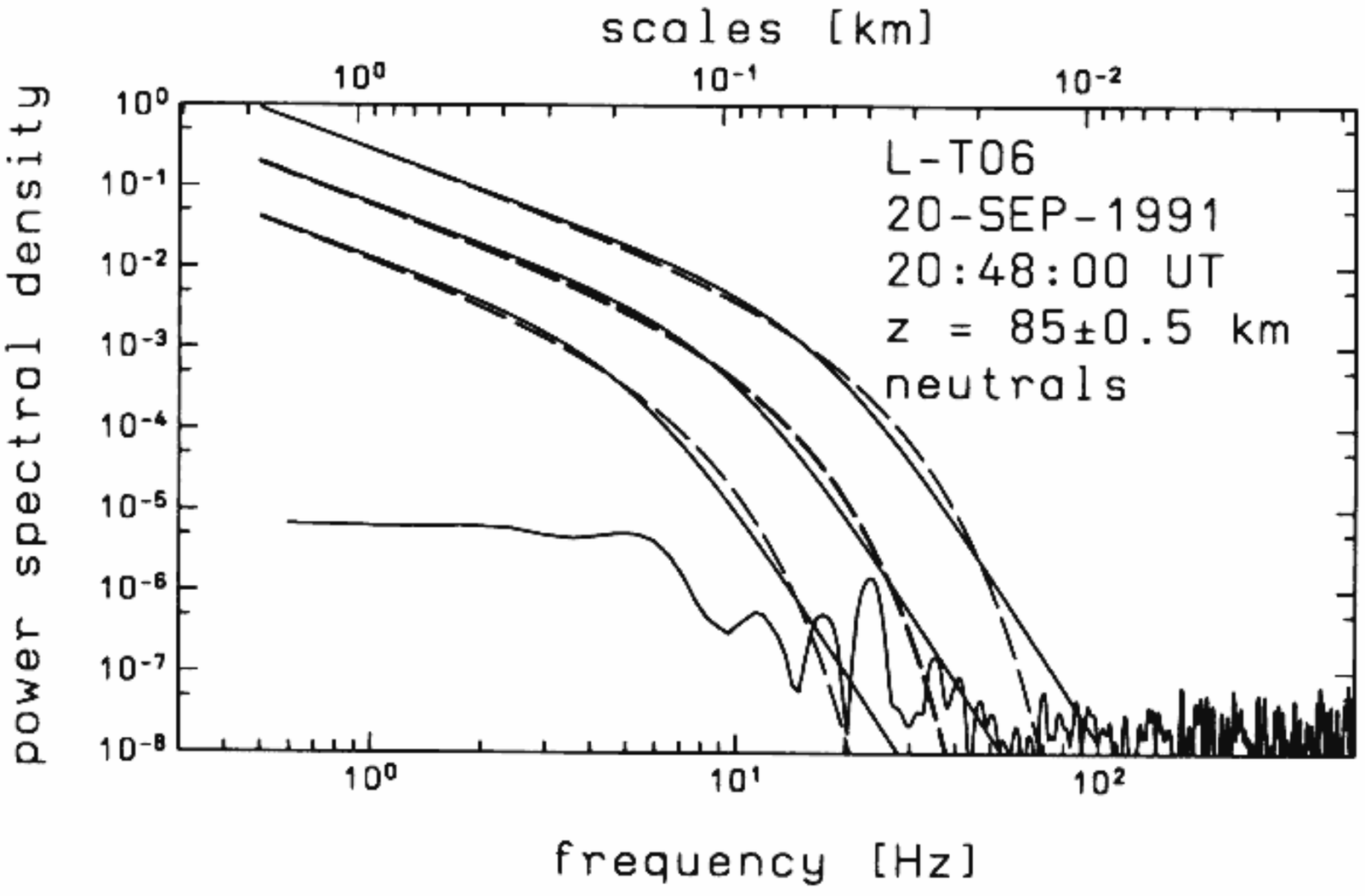

Fig. 5. Power spectrum of the residuals of Figure 3 (lower panel) together with theoretical spectra expected for energy dissipation rates of 10, 100, and 1000 mW kg^{-1}. The models from Heisenberg (solid line) and Tatarskii (dashed line) are shown. The variability dissipation rate N_n needed to calculate the theoretical spectra is taken from the spectrum in Figure 4. It is also varied by a factor of 10 (see text). The upper scale shows the spatial scales derived from $L \equiv \lambda = 2\pi/k = v_R/f$ (f = frequency; v_R = rocket velocity = 962 m s^{-1}).

TABLE 2. Turbulent Parameters Derived From the Spectrum in Figure 4

Parameters	Symbols and Units	Value
Altitude range, km		79 ± 2.5
Neutral density	n, m^{-3}	4.1×10^{20}
Temperature	T, K	196.
Kinematic viscosity	ν, m^2 s^{-1}	0.82
Brunt-Väisälä period	P_B, min	4.8
Mean gradient of $\Delta n/n$	M_n, l m^{-1}	4.9×10^{-5}
Original sampling frequency	Hz	4884.81
Effective frequency resolution	Δf, Hz	0.14895
Rocket velocity	v_r, m s^{-1}	977.
Inner scale (Heisenberg)	l_0^H, m	24.9
Inner scale (Tatarskii)	l_0^T, m	17.8
Energy dissipation rate	ϵ, mW kg^{-1}	13.8
Inhomogeneity dissipation rate	N_n, s^{-1}	$2.05_{\pm 0.4} \times 10^{-7}$
Heating rate	K d^{-1}	1.2
Kolmogoroff microscale	η, m	2.5
Structure function constant	C_n^2, m$^{-2/3}$	1.48×10^{-6}
Turbulent velocity	w_{turb}, m s^{-1}	1.1
Outer scale	L_B, m	359.
Turbulent diffusion coeff. for momentum	K_m, m^2 s^{-1}	14.

The summer mean profile in Figure 7 (from NLC-91) shows some interesting differences from the winter profiles (we should not forget, however, that only two flights contributed to this mean). Turbulence is practically absent

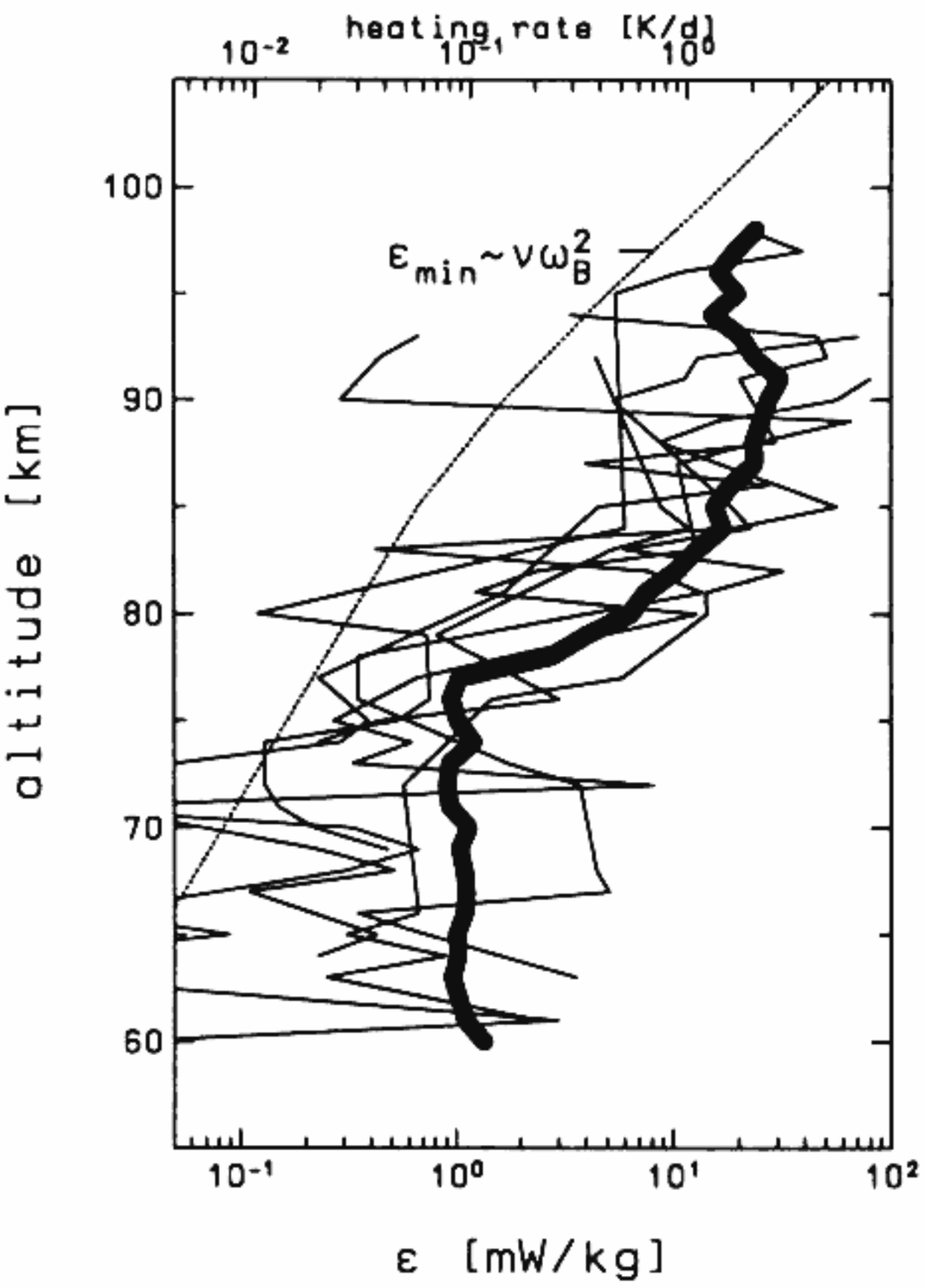

Fig. 6. Six energy dissipation rate profiles measured by the TOTAL instrument during the DYANA campaign in Andøya (69°N). The thick solid line represents the running mean over 5 km. The upper scale gives the corresponding heating rates in Kelvins per day. The dotted line presents a theoretical estimate of the lower limit for ϵ, obtained from $\epsilon_{\text{min}} = \nu\omega_B^2$.

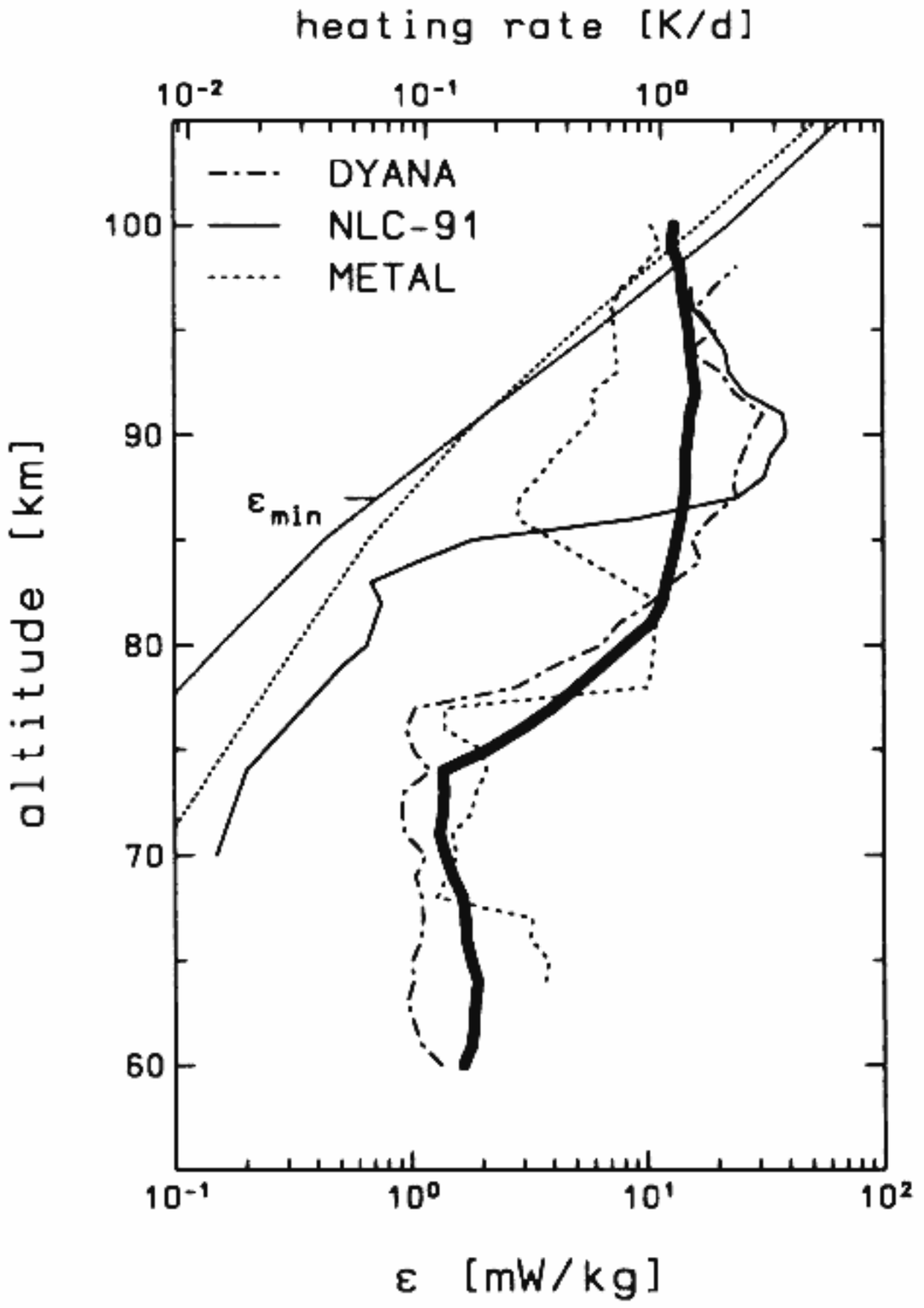

Fig. 7. Comparison of mean energy dissipation rate profiles obtained with TOTAL at high latitudes during three campaigns: DYANA in February/March 1990, NLC-91 in August 1991 and METAL in September/October 1991. The profile marked "ϵ_{min}" presents the expected lower limit for ϵ, derived from theory. Two ϵ_{min} profiles are shown for comparison: one for March and one for August.).

below 82 km and increases strongly above. This increase is mainly due to the high energy dissipation rates obtained during flight NBT05. It turned out that this turbulence layer coincided with the altitude where polar mesosphere summer echoes (PMSE) were detected by two VHF radars. For the first time this gave the chance to intercompare in situ measurements of neutral and plasma turbulence with the radar echoes. Results of this study are presented by *Lübken et al.* [1993*b*].

In Figure 8 the turbulent diffusivities for momentum K_m (equation (7)) and mean vertical turbulent velocities w_{turb} (equation (8)) are shown. Again, all our 14 TOTAL measurements at high latitudes are summarized in this plot. The mean turbulent diffusivities for momentum shown in Figure 8 are on the order of 5 m^2 s^{-1} in the lower mesosphere increasing to typical values of 70 m^2 s^{-1} in the upper mesosphere. Similar to the energy dissipation rates in Figure 7, the turbulent velocities and the turbulent diffusion coefficients were averaged, smoothed by a 5-point running mean and listed in Table 3. The turbopause is commonly defined as the altitude where the turbulent diffusion coefficient equals the molecular diffusion coefficient. Using this definition, we find the turbopause in an altitude of ~100 km. The mean vertical turbulent velocities shown in Figure 8 are of the order of 0.5–1 m s^{-1} in the entire mesosphere.

TABLE 3. Mean Turbulent Parameters Obtained by TOTAL During Winter Season at Andøya, 69°N

z, km	ε, mW kg^{-1}	w'_{turb}, m s^{-1}	K, m^2 s^{-1}
60.0	1.66	0.34	4.01
61.0	1.81	0.35	4.52
62.0	1.84	0.35	4.64
63.0	1.87	0.35	4.76
64.0	1.91	0.36	4.94
65.0	1.79	0.35	4.71
66.0	1.71	0.34	4.58
67.0	1.70	0.33	4.51
68.0	1.65	0.32	4.40
69.0	1.50	0.31	3.96
70.0	1.39	0.31	3.63
71.0	1.32	0.31	3.39
72.0	1.36	0.32	3.54
73.0	1.38	0.32	3.52
74.0	1.36	0.33	3.50
75.0	2.11	0.37	4.97
76.0	2.95	0.42	6.74
77.0	3.98	0.48	9.11
78.0	5.07	0.54	11.57
79.0	6.41	0.63	17.11
80.0	8.10	0.77	28.14
81.0	10.35	0.92	39.35
82.0	11.65	1.02	48.23
83.0	12.14	1.07	51.91
84.0	12.82	1.11	54.11
85.0	13.42	1.12	54.99
86.0	13.98	1.13	53.65
87.0	14.45	1.12	52.95
88.0	14.69	1.11	54.57
89.0	14.56	1.09	54.98
90.0	15.04	1.13	60.11
91.0	15.31	1.19	69.19
92.0	16.19	1.22	72.49
93.0	15.74	1.22	70.49
94.0	15.36	1.22	66.85
95.0	15.11	1.21	63.22
96.0	14.65	1.17	53.94
97.0	14.13	1.16	47.26
98.0	13.95	1.15	42.20
99.0	12.81	1.09	30.81
100.0	13.09	1.08	25.82

5. Comparison With Other Measurements and Models

We will now compare our TOTAL results with other measurements and with models. We will start with an intercomparison of turbulent energy dissipation rates, since this is the most direct measured quantity in our method (apart from l_0^H). Other parameters, as for example the turbulent diffusion coefficients or the turbulent velocities, require additional inputs from measurements (e.g., wind shears) or from theory (e.g., Richardson numbers).

Energy Dissipation Rates: Comparison With Other Measurements and With CIRA-1986

A detailed intercomparison of results obtained by TOTAL and PIP was performed for the flights during DYANA [*Lübken et al.*, 1993*a*]. Very good agreement between both mean ε profiles was found which gives us further confidence in the reliability of the technique. In Figure 9 we present a comparison of our TOTAL ε measurements at Andøya during DYANA and METAL with results obtained by an earlier version of the PIP instrument employed at the same location but during earlier winter campaigns: Energy Budget Campaign (EBC), Middle Atmosphere Program/Winter in Northern Europe (MAP/WINE) and Middle Atmosphere Cooperation, EPSILON (the name stems from the symbol used for the energy dissipation rate ε) (MAC/EPSILON). These campaigns took place in the winters of 1980/1981, 1984/1985 and 1987/1988 with a total of three, seven, and five flights, respectively [*Thrane et al.*, 1985; *Lübken et al.*, 1987; *Blix et al.*, 1990*b*]. For the EBC data, the u_z method was used for data reduction, which seems to give similar values as the structure function constant method, provided the constant recommended by *Blix et al.* [1990*a*] are used. The data in Figure 9 (crosses) are the mean of the three profiles measured during EBC. The data obtained during the MAP/WINE campaign were derived applying the structure function constant method, however, with a different set of constants than those recommended by *Blix et al.* [1990*a*]. They have therefore been reanalyzed using Blix's constants. In addition, they were smoothed by a 5-point equal weight running mean, similar to the TOTAL data. In the lower mesosphere (below 72 km) the PIP data seem to suggest higher ε values than TOTAL. We would like to point out, however, that the old version of the PIP instrument gave somewhat uncertain results at these altitudes, mainly because of decreasing ion densities and increasing instrumental noise effects. We therefore believe that the difference between TOTAL and PIP in the lower mesosphere is not a geophysical effect but is instead caused by instrumental uncertainties of the old PIP sensor. The performance of PIP has significantly been improved since then.

It is evident from Figure 9 that all measurements at high latitudes (PIP and TOTAL) suggest low energy dissipation rates in the upper mesosphere. Please note that a total of 27 (= 3 + 7 + 5 + 6 + 6) flights performed in five different campaigns are summarized in that figure.

We now come to the comparison of TOTAL results with measurements other than those performed by PIP. We will not consider our summer mean profile from NLC-91 for comparison, since only two flights contributed to that mean. As noted earlier, only a few measurements of turbulent parameters have been performed in the past, especially when we concentrate on high latitudes. A summary of most of the measurements available before 1985 is presented in CIRA-1986 [*Hocking*, 1990]. Concerning high latitudes (51°–90°), all measured profiles are from *Zimmerman and Murphy* [1977] or from *Manson et al.* [1980, 1981]. The mean profile deduced from these measurements for winter is reproduced in Figure 10 (thick dashed line). The ε values are more than 1 order of magnitude larger than our TOTAL results. *Zimmerman and Murphy* [1977] used rocket grenade temperatures and horizontal winds. The energy dissipation rates that they derived include uncertainties which are basically related to the poor spatial resolution of the original data (3–6 km) which is not sufficient to exclude nonturbulent processes. Concerning the MF radar measurements at high latitudes, autocorrelation measurements (which are related to the radar spectral width) and irregular wind variabilities were used. The problem with this technique is that nonturbulent processes, such as beam broadening and shear broadening, significantly contribute to the spectral width and have to be accounted for in the data reduction before the turbulent signal is deduced [*Hocking*, 1983]. In addition, the background gradient of the potential refractive index M_n is

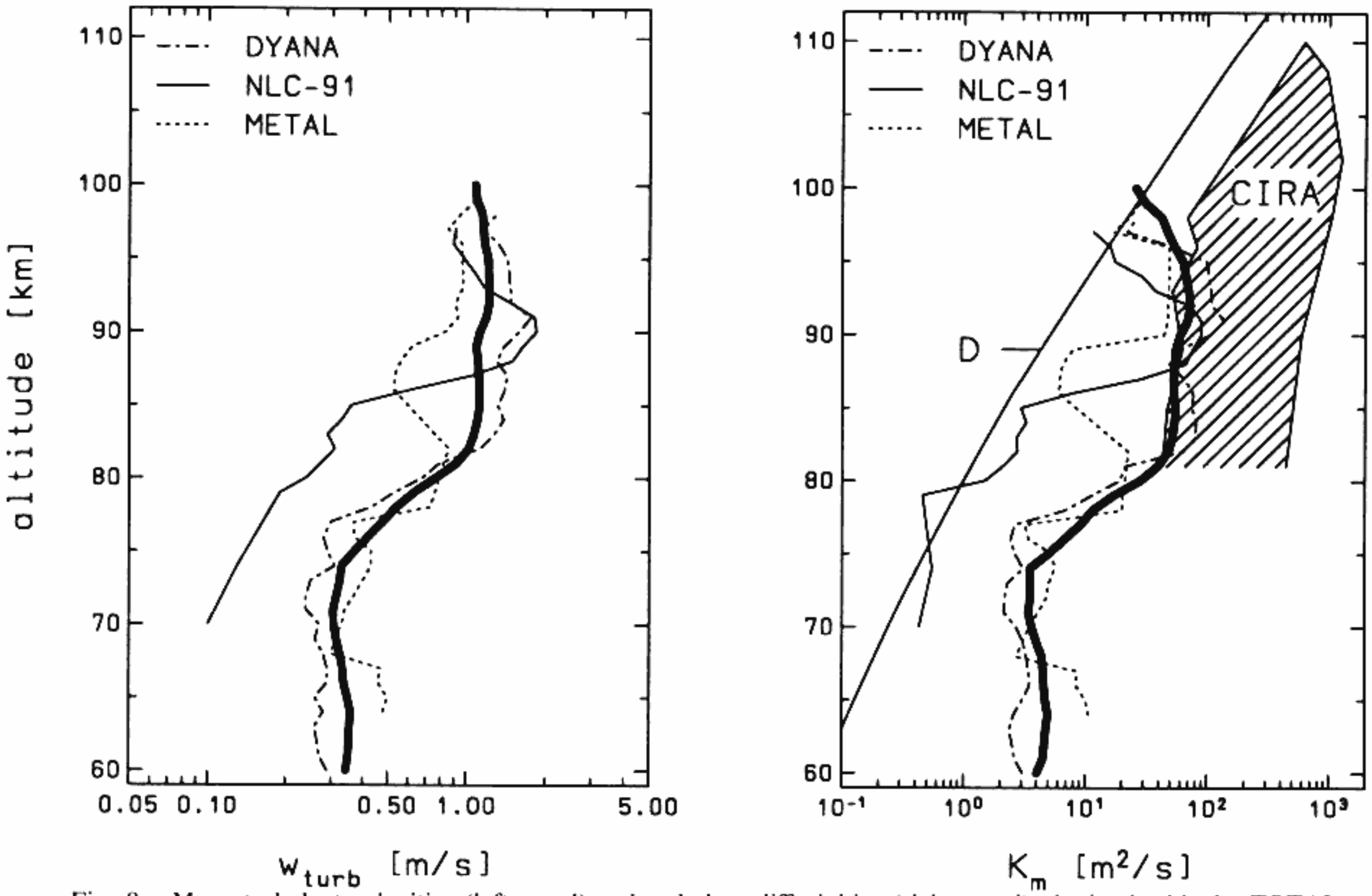

Fig. 8. Mean turbulent velocities (left panel) and turbulent diffusivities (right panel) obtained with the TOTAL instrument at high latitudes for three campaigns: DYANA in February/March 1990, NLC-91 in August 1991 and METAL in September/October 1991. For comparison, the molecular diffusion coefficient D and the CIRA-1986 empirical model [*Hocking*, 1990] are also shown.

needed in order to deduce quantitative results from the spectral width [*Hocking*, 1985]. M_n itself depends on temperature, neutral and electron number density, which are normally not measured but are taken from empirical models. Significant uncertainties are introduced if the actual atmospheric parameters deviate from the models. It appears therefore that radars provide only a rough estimate of turbulent parameters which, because of nonturbulent effects, have a tendency for too large absolute values. We suspect that the large values of the high-latitude winter CIRA-1986 profile are caused by instrumental effects.

In Figure 10 we have also reproduced the 67% range of global energy dissipation rates from CIRA-1986 (see *Hocking* [1990] for more details on the database and the averaging procedure). Again, the mean profile deduced from our TOTAL measurements is significantly smaller than this compilation (hatched area in Figure 10). Most of the measurements contributing to the global profile stem from chemical releases or from MF radar techniques, which, as has been explained above, are uncertain due to nonturbulent processes and/or unknown background parameters. None of the profiles contributing to CIRA-1986 stems from neutral density fluctuation measurements.

In Table 4, all winter measurements of ε profiles at high latitudes (51°–90°) are listed, both for periods before and after CIRA-1986. Most of the profiles were obtained after CIRA-1986, especially when we summarize the autumn and winter measurements: seven profiles are contained in CIRA-1986 and 40 were measured later. Furthermore, new techniques have been employed which are not presented in CIRA-1986, for example, our neutral fluctuation measurements. Apart from the TOTAL and PIP data, there are three more data sets published in the literature for high latitudes, which are also shown in Figure 10: the foil cloud results [from *Wu and Widdel*, 1989] (dotted-dashed line), the radar data [from *Hocking*, 1986] (two dots), and the chaff dispersion results as described below. *Wu and Widdel* [1989] used their foil cloud technique to obtain spectra from small-scale vertical wind fluctuations. The spectra were integrated between the outer scale L_B (they used a fixed value L_B = 600 m) and the inner scale. The integral was then taken as a measure of the mean turbulent velocity w_{turb}. Finally, energy dissipation rates were derived using Weinstock's equation (see equation (8)). The difficulty with this method is that the radar noise simulates motions of the foil cloud, especially at small scales. In addition, the outer scale is the critical parameter when integrating the spectrum and cannot be treated as a fixed constant but depends itself on ε. Despite these uncertainties, the profile of mean energy dissipation rates derived from a maximum of 12 flights (data coverage depends on altitude) seems to agree roughly with TOTAL in the lower mesosphere but decreases to very small values above 80 km. The two dots in Figure 10 (left panel) are from *Hocking* [1986], who applied the analysis technique discussed by *Hocking* [1983] to the SOUSY VHF radar data collected during two days in October 1981 in the Harz mountains, in Germany. The lower altitude (70 km) value is very close to our mean. The second value at 78 km is significantly larger compared to our mean, but the radar value is an upper limit as is explained by *Hocking* [1983].

The chaff dispersion technique was employed during MAP/WINE, MAC/EPSILON and DYANA at Heiss Island (81°N, 58°E) and Volgograd (48°N, 44°E) and gives a time series of ε data around 75 km. The results are described in

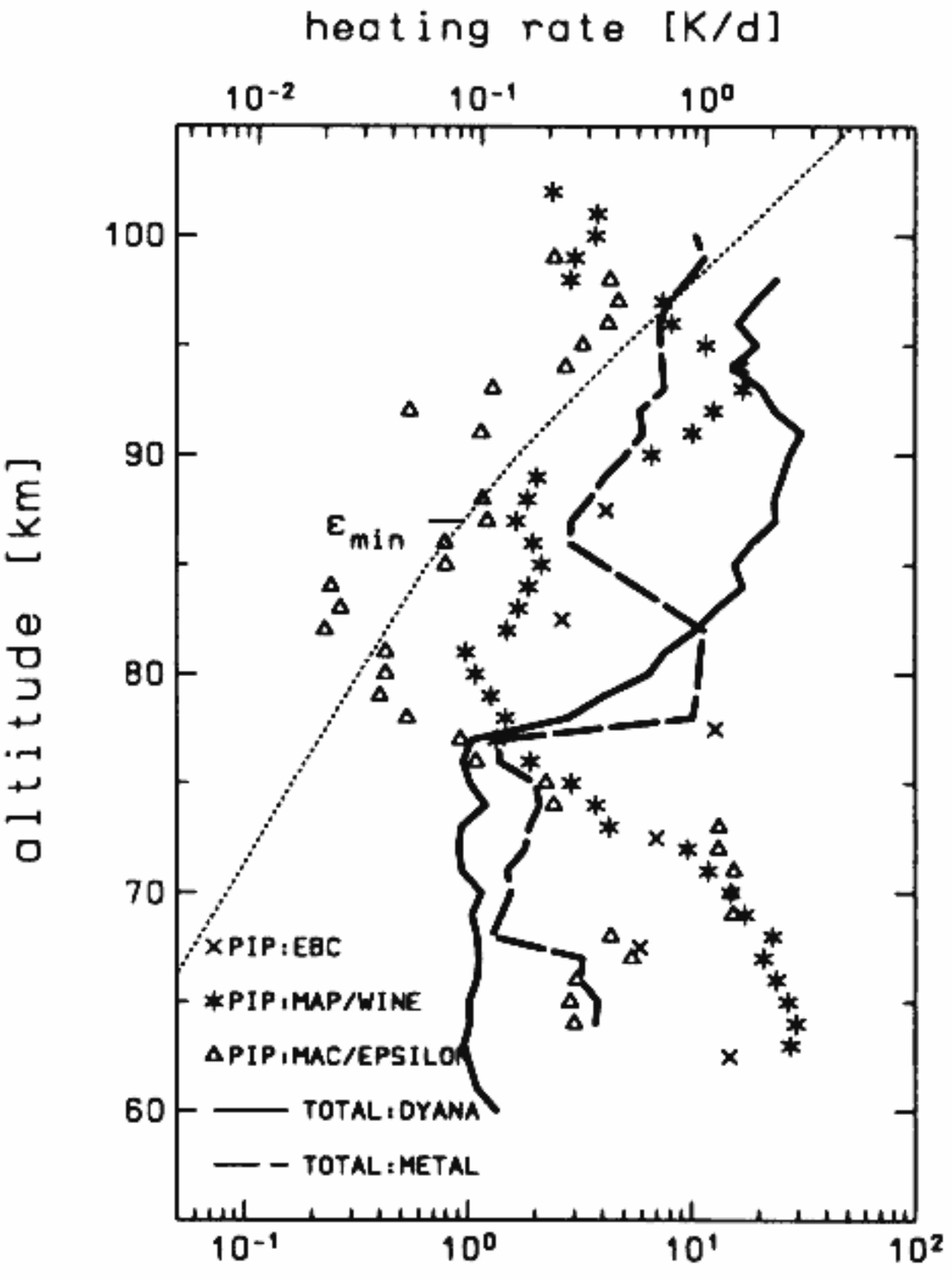

Fig. 9. Comparison of mean energy dissipation rates obtained with TOTAL during winter (DYANA and METAL) with measurements by PIP during earlier campaigns. All measurements shown were performed in Andøya. More information about the campaigns is given in the text.

the turbulence papers of these campaigns [*Lübken et al.*, 1987; *Blix et al.*, 1990*b*; *Lübken et al.*, 1993*a*]. The range of measurements is shown in Figure 10 as a box labeled "Chaff." The energy dissipation rates measured by this technique are considerably larger than ours because they present upper limits due to nonturbulent dispersion processes.

Summarizing the situation in the high-latitude winter, most of the measurements performed after CIRA-1986 are from TOTAL and PIP. They suggest that the CIRA-1986 winter profile is too high by at least 1 order of magnitude. Furthermore, our TOTAL results are also considerably smaller when compared with the range of global ε values presented in CIRA-1986 (hatched area in Figure 10).

Energy Dissipation Rates: Comparison With Models

In Figure 11 we compare our TOTAL results with the models of *Chandra* [1980], *Gordiets et al.* [1982], *Ebel et al.* [1983], and D. C. Fritts and T. VanZandt (Spectral estimates of gravity wave energy and momentum fluxes, I, Energy dissipation, acceleration, and constraints, submitted to *Journal of the Atmospheric Sciences*, 1993) (hereinafter referred to as D. C. Fritts and T. VanZandt, unpublished manuscript, 1993). It is obvious from Figure 11 that all models show significantly higher ε values compared to our measurements: whereas the models arrive at typically 100 mW kg^{-1} in the upper mesosphere, the TOTAL mean values are of the order of 10 mW kg^{-1} in that altitude range. We will later discuss the consequences of this difference. We would like to mention, however, that the model results critically depend on certain parameters (e.g., the critical flux Richardson number introduced later) which are not known. The values advertised by D. C. Fritts and T. VanZandt (unpublished manuscript, 1993) were based on canonical wave forcing at lower levels. Implementation of this scheme in the NCAR TGCM suggests that somewhat smaller wave energies are appropriate (D. C. Fritts, private communication, 1993). Additionally, it should be kept in mind that these values represent an upper limit because of other dissipation processes not included in the model.

In general, it should be noted that turbulence in models is not determined in a self-consistent manner but is regarded as a means to compensate for deficiencies in the momentum and/or heat budget. The treatment of turbulence in models is always speculative, and parameterizations derived from observations are often used. It is the purpose of this paper to show that the parameterizations used in the literature probably overestimate turbulent heating.

Turbulent Diffusivities: Comparison With CIRA-86

We now come to a comparison of our mean TOTAL turbulent diffusion coefficients K with the CIRA-1986 empir-

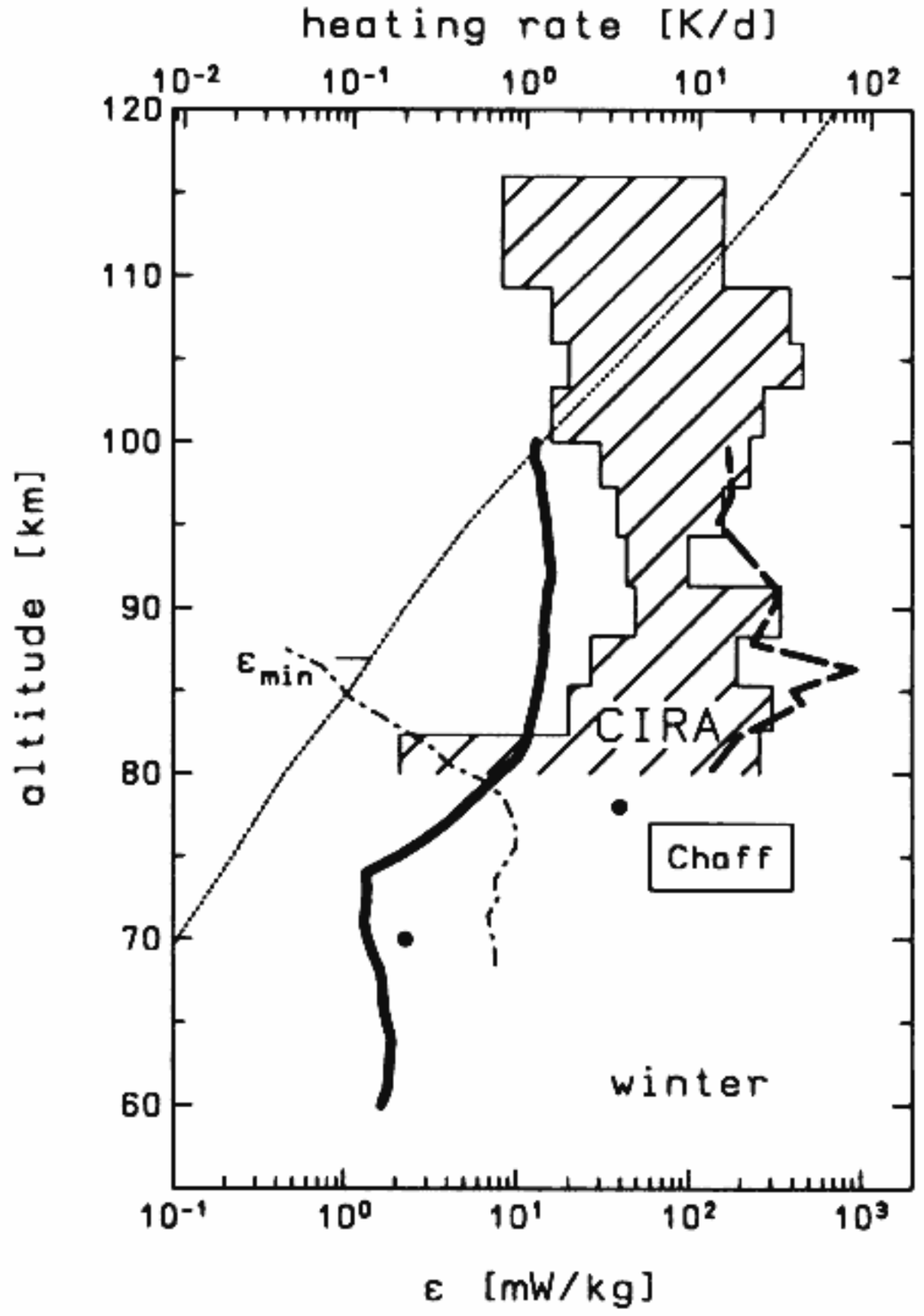

Fig. 10. Comparison of mean energy dissipation rates from TOTAL (thick solid line) during winter with CIRA-1986 (thick dashed line) and with other measurements, except PIP which has already been discussed. The hatched area shows the range of global ε measurements between 16th and 84th percentile from CIRA-1986 [*Hocking*, 1990]. The dotted-dashed profile stems from the foil cloud technique, and the two dots are from the SOUSY radar. The box labeled "Chaff" represents the range of measurements from the Russian chaff dispersion technique.

TABLE 4. List of All Measurements of Turbulent Energy Dissipation Rate Profiles Performed at High Latitudes (51°–90°)

Reference	Site	Number Profiles in Sp	So	Au	Wi	Method	Campaign	Year
		Included in CIRA-1986						
Zimmerman and Murphy [1977]	Point Barrow		1		1	rocket grenade		1965/1967
	Fort Churchill		1		1			
Manson et al. [1980, 1981]	Saskatoon		1		1	radar		1977/1978
		1	1	2	2			1978/1979
Sum (total = 12)		1	4	2	5			
		Not Included in CIRA-1986						
Hocking [1986]	Harz			1		radar		1981
Thrane et al. [1985]	Andøya			3		$\Delta N_i/N_i$	EBC	1980/1981
Watkins et al. [1988]	Poker Flat		2			radar	STATE	1983
Lübken et al. [1987]	Andøya			7		$\Delta n/n$; $\Delta N_i/N_i$	WINE	1984/1985
Wu and Widdel [1989]	Andøya			12		foil cloud	WINE	1984/1985
Kelley et al. [1990]	Andøya	1				$\Delta N_e/N_e$	SINE	1987
Blix et al. [1990*b*]	Andøya		5			$\Delta n/n$; $\Delta N_i/N_i$	EPSILON	1987/1988
Lübken et al. [1993*a*]	Andøya			6		$\Delta n/n$; $\Delta N_i/N_i$	DYANA	1990
(this study)	Kiruna	2				$\Delta n/n$; $\Delta N_i/N_i$	NLC-91	1991
(this study)	Andøya		6			$\Delta n/n$; $\Delta N_i/N_i$	METAL	1991
Sum (total = 45)		5	15	25				

The parameters $\Delta n/n$, $\Delta N_i/N_i$, and $\Delta N_e/N_e$ are relative neutral, ion and electron density fluctuations, respectively. More details about the campaigns and the techniques employed can be found in the references listed.

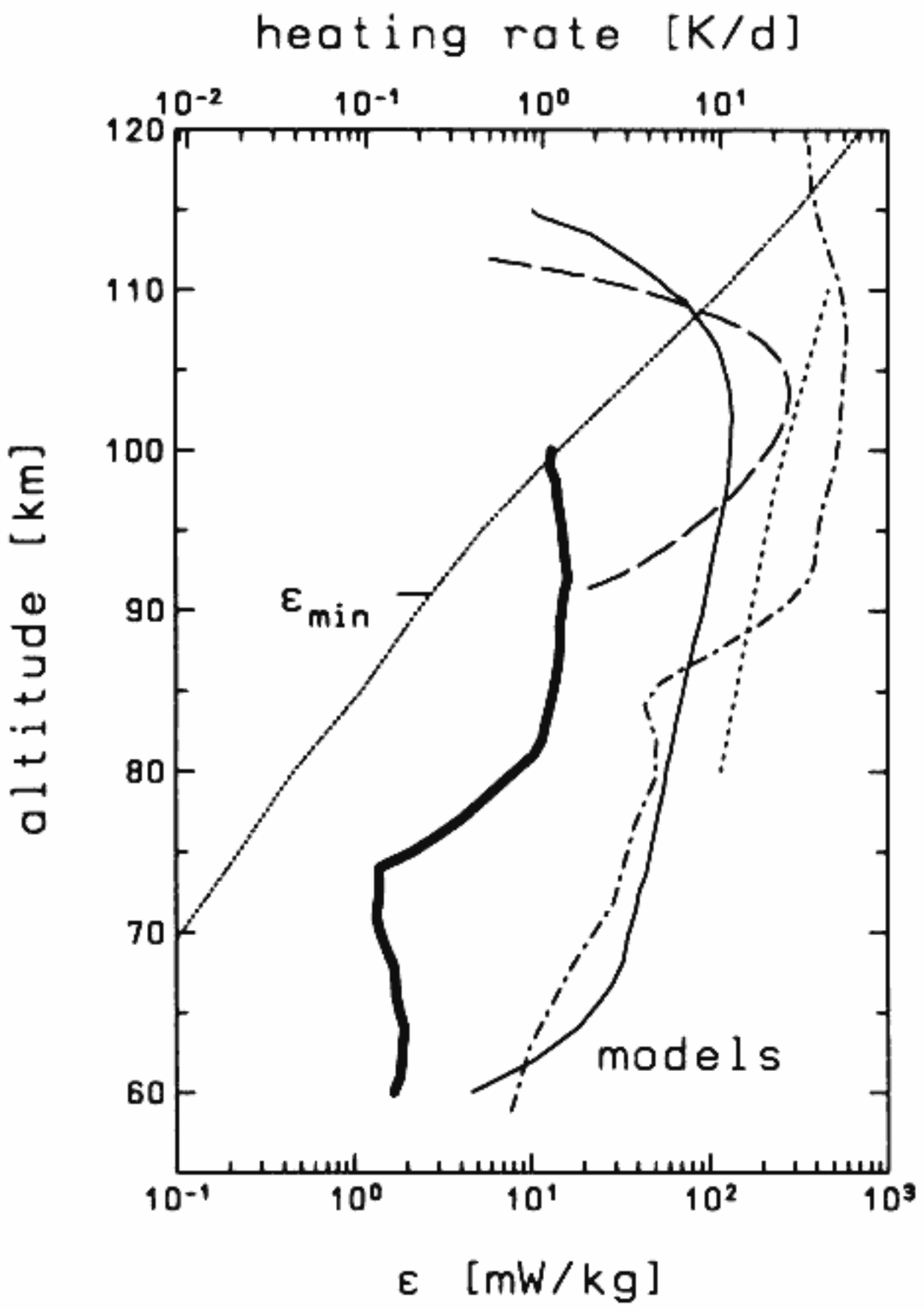

Fig. 11. Comparison of mean energy dissipation rates measured by the TOTAL instrument during winter at high latitudes (thick solid line) with the following models: *Chandra* [1980] (denoted by thin solid line), *Gordiets et al.* [1982] (denoted by dashed line), *Ebel et al.* [1983] (denoted by dotted line), and D. C. Fritts and W. Lu (Spectral estimates of gravity wave energy and momentum fluxes, II, Parameterization of wave forcing and variability, submitted to the *Journal of Atmospheric Sciences*, 1993) (denoted by dot-dashed line). The models are described in more detail in the text. All model profiles show significantly larger ε values compared to our measurements. The dotted line presents a theoretical estimate of the lower limit for ε.

ical model [*Hocking*, 1990]. This comparison is more problematic than that of ε because the physical process described by K may be different for different measurements, and what makes a comparison even more difficult is that the transfer from one measurement of K to another may be vague, if not impossible. For example, when we try to link small-scale turbulent mixing processes to the net effect of turbulence on the mixing ratio of an inert gas, we need to take into account the timescales involved, spatial anisotropy, and temporal intermittency. Furthermore, processes may affect the mixing ratio which are not related to turbulence at all, for example, vertical bulk motions. We have to keep in mind these limitations when we compare our results with other measurements. In Figure 8 we show the compilation of eddy diffusion coefficients of CIRA-1986 together with our mean profiles. Concentrating on the winter mean of our data (thick solid line), we find that (as with the energy dissipation rates) our measurements show significantly smaller values than CIRA-1986; however, the difference is not as large as for ε.

An analytical profile of $K(z)$ is presented in the United States Standard Atmosphere 1976 (USSA-1976):

$$K_e(z) = K_0 \exp\left(1 - \frac{a}{a - (z - z_0)^2}\right) \qquad (13)$$

where the values used in USSA-1976 are $K_0 = 120$ m^2 s^{-1}; $a = 400$ km^2, and $z_0 = 95$ km. We have adjusted this profile to the TOTAL mean profile and arrive at the following parameters: $K_0 = 60$ m^2 s^{-1}; $a = 300$ km^2, and $z_0 = 88$ km.

6. Discussion

A direct consequence of our experimental result is that the contribution of turbulent heating to the energy budget can be neglected compared to the prevailing terms. In the notation of *Chandra* [1980] the heat balance equation in the middle and upper atmosphere can be written as

$$\Sigma \rho_i C_{p,i} \frac{dT}{dt} - \frac{dp_i}{dt} = Q_{\mathrm{EUV}} + Q_{\mathrm{UV}} + Q_{\mathrm{Ch}} - Q_{\mathrm{IR}} + \rho\varepsilon - \frac{\partial}{\partial z}(F_{m,h} + F_{t,h}) \quad (14)$$

where ρ_i, $C_{p,i}$ and p_i are the density, pressure, and specific heat at constant pressure of the ith constituent; Q_{EUV}, Q_{UV}, Q_{Ch} and Q_{IR} are the heating and cooling rates due to solar radiation (EUV and UV), exothermal chemical reactions and radiative processes, respectively. We now want to discuss the consequences of our result for this balance. We should keep in mind, however, that (14) describes global long-term variations and may not be applicable locally in all cases. Our TOTAL measurements indicate, that the term $\rho\varepsilon$ on the right-hand side of equation (14) can be neglected (the importance of the various terms in equation (14) varies with height).

What do our experimental results contribute to the question whether turbulence heats or cools the atmosphere? A premature expectation might be that turbulence should be a cooling process when the heating due to ε is very small. However, if very little turbulence is present, the turbulent heat flow, which determines the cooling effect of turbulence, is also very small. We need to be more precise and consider turbulent heating versus cooling efficiency in more detail. As shown by *Zimmerman and Keneshea* [1986], the ratio of turbulent heating to cooling rates is given by

$$\mathrm{Ratio} = \frac{\text{cooling}}{\text{heating}} = \frac{\text{divergence of turbulent heat flux}}{\text{turbulent energy dissipation}} = \frac{7}{2}\frac{R_{fc}}{1 - R_{fc}} = \frac{7}{2}\alpha_{fc} \quad (15)$$

where R_{fc} is the critical flux Richardson number. As can be seen from equation (15), it is this parameter (or alternatively α_{fc}, as used by *Chandra* [1980]) which determines, whether turbulence heats or cools the atmosphere. We should mention, however, that some assumptions have been made in deriving the above relationships which may not always be justified (for example, some terms may have to be supplemented to the turbulent energy budget equations as discussed by *Ebel et al.* [1983]). We will now show that we do not have to speculate about the appropriate value for R_{fc} because it is no longer relevant for the role of turbulence in the heat budget, provided ε is small. The reason for this is that the terms in the turbulent energy equation are interrelated. This means that a small value for ε implies small values for the other terms too. In its simplest form, the turbulent energy equation can be written as (assuming steady state conditions)

$$e_s = \varepsilon + e_g \quad (16)$$

where e_s is the extraction of energy from wind shear and e_g is the work done against buoyancy. The latter can be written as

$$e_g = -\frac{g}{T}\langle w'T'\rangle = \frac{g}{T}K_T\left(\frac{\partial T}{\partial z} - \Gamma\right) = K_T\omega_B^2 \quad (17)$$

Using the definition of the Prandtl number ($Pr_T^{\mathrm{tur}} \equiv K_m/K_T$) and the relationship between K_m and ε presented by *Weinstock* [1978*b*], we arrive at

$$e_g = \frac{0.81}{Pr_T^{\mathrm{tur}}}\varepsilon \quad (18)$$

Thus if ε is very small, the work done by turbulence against buoyancy is also small, provided the turbulent Prandtl number Pr_T^{tur} is not much smaller than 1, which is unlikely according to current estimates published in the literature. Furthermore, from the turbulent energy budget it follows that the shear production term e_s must be small too. We summarize that a small ε value implies small values for e_g and e_s. This result can now be used to show that the cooling by turbulent heat conduction is also small. This cooling rate is given by the divergence of the turbulent heat flux. The corresponding expression can be further simplified (see *Zimmerman and Keneshea* [1986] for more details):

$$\left(\frac{\partial T}{\partial t}\right)_c = \frac{1}{\rho c_p}\frac{\partial}{\partial z}F_{h,t} = -\frac{\langle w'T'\rangle}{H_p} = -\frac{m}{k}\left(\frac{g}{T}\langle w'T'\rangle\right) = \left(-\frac{m}{k}\right)e_g = \left(-\frac{7}{2c_p}\right)e_g = \frac{0.245}{Pr_T^{\mathrm{tur}}}\varepsilon[K/d] \quad (19)$$

where ε is given in watts per kilogram.

Since e_g is small, the cooling effect by turbulence heat conduction is also small. If we take $\varepsilon = 10$ mW kg^{-1} as a typical value from TOTAL in the upper mesosphere, we arrive at $(\partial T/\partial t)_c = 2.4$ K d^{-1}, assuming $Pr_T^{\mathrm{tur}} = 1$. Thus not only can we neglect the term $\rho\varepsilon$ in (14), but also the term $\partial/\partial z\, F_{t,h}$ (assuming that the prevailing terms are of the order of 10–20 K d^{-1}).

In summary, whether or not the ratio of turbulent heating to cooling is larger or smaller than unity is irrelevant because in absolute terms, both contributions to the heat budget of the upper atmosphere are small.

Assuming that our measurements are typical for the upper atmosphere in general, we conclude that the role of turbulence for the heat budget in the upper atmosphere is much less important than commonly believed in the literature. This experimental result gains further importance when regarding the very recent finding that the cooling efficiency of CO_2 is presumably much larger than thought before due to a larger deactivation rate coefficient of CO_2 by atomic oxygen [*Sharma and Wintersteiner*, 1990; *Shved et al.*, 1991]. The new deactivation rate gives a cooling rate for the lower thermosphere which is 2–3 times the rate previous calculated. This result was confirmed by the ATMOS satellite observations of upper atmospheric CO_2 (ν_2) vibrational temperatures which suggest very high cooling rates induced by CO_2 [*Lòpez-Puertas et al.*, 1992]. Carbon dioxide can therefore account for much of the cooling formerly attributed to turbulence. This is not only important for the Earth's atmosphere but also for other terrestrial planets, in particular for the Venus thermosphere (remember that the Venus atmosphere consists to 96.5% of carbon dioxide). The new cooling rates of carbon dioxide can explain the puzzling problem of the very low temperatures of the nightside thermosphere of Venus (it was speculated that these low temperatures could be attributed to cooling by turbulent heat conduction) [*Gordiets and Kulikov*, 1985].

7. SUMMARY

In summary, the most important results of this study are given below.

1. The TOTAL instrument is capable of detecting very small scale neutral density fluctuations in the mesosphere and lower thermosphere. It achieves an unprecedented spatial resolution (approximately 1 m) concerning neutral atmosphere structures in the mesosphere. The TOTAL instrument on board the TURBO payload was flown 17 times in the years 1990/1991. All flights were successful and gave scientific results. We concentrate on the 12 flights performed under winter conditions at high latitudes (69°N).

2. A recently developed method to deduce geophysically relevant turbulent parameters from the TOTAL number density fluctuation measurements was applied making use of the very high spatial resolution achieved by TOTAL. The new method considerably improves the reliability of the quantitative results. Typical relative uncertainties of the turbulent parameters (e.g., energy dissipation rate ε) are 50% only (but note the discussion after equation (9)).

3. The TURBO flights were accompanied by nearly simultaneous measurements of atmospheric background parameters, which further improve the reliability of the derived turbulent parameters.

4. Turbulence was detected by TOTAL in distinct layers of a few kilometers' thickness. Between these layers the atmosphere was normally found to be very quiet. The atmospheric background parameters measured simultaneously showed that turbulence is frequently observed in regions of instabilities with correspondingly low gradient Richardson numbers.

5. The mean of the 12 high-latitude winter flights showed very small turbulent energy dissipation rates ε of ~2 mW kg^{-1} in the lower mesosphere (60–75 km) and ~10–20 mW kg^{-1} in the upper mesosphere and lower thermosphere (80–100 km). The corresponding heating rates are 0.17 and ~1 K d^{-1}, respectively.

6. The mean turbulent energy dissipation rate profile obtained from our measurements is at least 1 order of magnitude smaller than is up to now believed to be typical in the mesosphere. The values are also smaller than typical experimental results obtained by other techniques (with much poorer spatial resolution) or results from model investigations.

7. Theoretical considerations involving the energy budget of turbulence show that not only is turbulent heating small, but so is cooling due to turbulent heat conduction.

Acknowledgments. We would like to thank our colleagues K.-H. Fricke and F. Föhner who supported the development of TOTAL and the scientific analysis of the results. The TOTAL instruments were built at the University of Bonn with major contributions on the mechanical details from H. Baumann. We would like to thank D. Offermann, E. Kopp, R. Goldberg, and G. Witt for initiating and successfully performing the DYANA and the NLC-91 campaign, respectively. We gratefully acknowledge the excellent support of the TURBO flights by the personnel from the following institutions: Andøya Rocket Range (Norway), Centre d'Essais des Landes (France), Mobile Raketenbasis (Germany) and Norwegian Defence and Research Establishment (Norway). The TURBO project was supported by the Bundesministerium für Forschung und Technologie, Bonn, under grant 010E88027.

REFERENCES

Blix, T. A., E. V. Thrane, and O. Andreassen, In situ measurements of fine scale structure and turbulence in the mesosphere and lower thermosphere by means of electrostatic positive ion probes, *J. Geophys. Res.*, *95*, 5533–5548, 1990*a*.

Blix, T. A., E. V. Thrane, D. C. Fritts, U. von Zahn, F.-J. Lübken, W. Hillert, S. P. Blood, J. D. Mitchell, G. A. Kokin, and S. V. Pakhomov, Small scale structure observed in situ during MAC/EPSILON, *J. Atmos. Terr. Phys.*, *52*, 835–854, 1990*b*.

Blix, T. A., E. V. Thrane, U. P. Hoppe, C. Hall, S. Kirkwood, J. Ulwick, and M. Friedrich, Plasma turbulence in the lower E-region observed during the DYANA campaign, *J. Atmos. Terr. Phys.*, in press, 1993.

Chandra, S., Energetics and thermal structure of the middle atmosphere, *Planet. Space Sci.*, *28*, 585–593, 1980.

Chapman, S., and T. G. Cowling, *The Mathematical Theory of Non-Uniform Gases*, Cambridge University Press, New York, 1970.

Coy, L., and D. C. Fritts, Gravity wave heat fluxes: A Lagrangian approach, *J. Atmos. Sci.*, *45*, 1770–1780, 1988.

Czechowsky, P., B. Inhester, J. Klostermeyer, R. Rüster, and G. Schmidt, Simultaneous radar and lidar observations during the DYANA campaign, in *Proceedings of the 10th ESA Symposium on European Rocket and Balloon Programmes and Related Research, Cannes-Mandelieu, France, Eur. Space Agency Spec. Publ. ESA SP-317*, 399–400, 1991.

Ebel, A., H. J. Jakobs, and P. Speth, Turbulent heating and cooling of the mesopause region and their parameterization, *Ann. Geophys.*, *1*, 359–370, 1983.

Fleming, E. L., S. Chandra, J. J. Barnett, and M. Corney, Zonal mean temperature, pressure, zonal wind and geopotential height as functions of latitude, *Adv. Space Res.*, *10*(12), 11–59, 1990.

Fricke, K. H., and U. von Zahn, Mesopause temperatures derived from probing the hyperfine structure of the D2 resonance line of sodium by lidar, *J. Atmos. Terr. Phys.*, *47*, 499–512, 1985.

Friker, A., and F.-J. Lübken, Neutral air density and temperature measurements by the TOTAL instrument aboard the ROSE payload, *J. Atmos. Terr. Phys.*, *54*, 693–701, 1992.

Fritts, D. C., and T. J. Dunkerton, Fluxes of heat and constituents due to convectively unstable gravity waves, *J. Atmos. Sci.*, *42*, 549–556, 1985.

Gärtner, V., and M. Memmesheimer, Computation of the zonally-averaged circulation driven by heating due to radiation and turbulence, *J. Atmos. Terr. Phys.*, *46*, 755–765, 1984.

Goldberg, R., E. Kopp, W. Swartz, and G. Witt, An overview of NLC-91, a rocket-radar campaign to study the polar summer mesosphere, *Geophys. Res. Lett.*, *20*, 2283–2286, 1993.

Gordiets, B. F., and Y. N. Kulikov, On the mechanisms of cooling of the nightside thermosphere of Venus, *Adv. Space Res.*, *5*, 113–117, 1985.

Gordiets, B. F., Y. N. Kulikov, M. N. Markov, and M. Y. Marov, Numerical modeling of the thermospheric heat budget, *J. Geophys. Res.*, *87*(9), 4504–4514, 1982.

Hauchecorne, A., and M. Chanin, Density and temperature profiles obtained by lidar between 35 and 70 km, *Geophys. Res. Lett.*, *7*, 565–568, 1980.

Heisenberg, W., Zur statistischen Theorie der Turbulenz, *Z. Phys.*, *124*, 628–657, 1948.

Hill, R. J., Models of the scalar spectrum for turbulent advection, *J. Fluid Mech.*, *88*, 541–562, 1978.

Hillert, W., F.-J. Lübken, and G. Lehmacher, Neutral air turbulence during DYANA as measured by the TOTAL instrument, *J. Atmos. Terr. Phys.*, in press, 1993.

Hocking, W. K., On the extraction of atmospheric turbulence parameters from radar backscatter Doppler spectra, I, Theory, *J. Atmos. Terr. Phys.*, *45*, 89–102, 1983.

Hocking, W. K., Measurement of turbulent energy dissipation rates in the middle atmosphere by radar techniques: A review, *Radio Sci.*, *20*, 1403–1422, 1985.

Hocking, W. K., Observation and measurement of turbulence in the middle atmosphere with a VHF radar, *J. Atmos. Terr. Phys.*, *48*, 655–670, 1986.

Hocking, W., Turbulence in the region 80–120 km, *Adv. Space Res.*, *10*(12), 153–161, 1990.

Hunten, D. M., Energetics of thermospheric eddy transport, *J. Geophys. Res.*, *79*, 2533–2534, 1974.

Johnson, F. S., Transport processes in the upper atmosphere, *J. Atmos. Sci.*, *32*, 1658–1662, 1975.

Jones, J., and J. W. Peterson, Falling sphere measurements 30 to 120 km, *Meteorol. Monogr.*, *8*, 176–177, 1968.

Justus, C. G., The eddy diffusivities, energy balance parameters, and heating rate of upper atmospheric turbulence, *J. Geophys. Res.*, *72*, 1035–1039, 1967.

Kelley, M. C., J. C. Ulwick, J. Röttger, B. Inhester, T. Hall, and T. Blix, Intense turbulence in the polar mesosphere: Rocket and radar measurements, *J. Atmos. Terr. Phys.*, *52*, 875–892, 1990.

Lòpez-Puertas, M., M. A. Lòpez-Valverde, C. P. Rinsland, and M. R. Gunson, Analysis of the upper atmosphere CO_2 (ν_2) vibrational temperatures retrieved from ATMOS/Spacelab 3 observations, *J. Geophys. Res.*, *97*, 20,469–20,478, 1992.

Lübken, F.-J., On the extraction of turbulent parameters from atmospheric density fluctuations, *J. Geophys. Res.*, *97*, 20,385–20,395, 1992.

Lübken, F.-J., and W. Hillert, Measurements of turbulent energy dissipation rates applying spectral models, in *Coupling Processes in the Lower Middle Atmosphere: NATO Advanced Research Workshop*, pp. 345–351, Kluwer Academic, Norwell, Mass., 1992.

Lübken, F.-J., and U. von Zahn, Thermal structure of the mesopause region at polar latitudes, *J. Geophys. Res.*, *96*, 20,841–20,857, 1991.

Lübken, F.-J., U. von Zahn, E. V. Thrane, T. Blix, G. A. Kokin, and S. V. Pachomov, In situ measurements of turbulent energy dissipation rates and eddy diffusion coefficients during MAP/WINE, *J. Atmos. Terr. Phys.*, *49*, 763–775, 1987.

Lübken, F.-J., T. Blix, U.-P. Hoppe, Knyazev, Kokin, G. Lehmacher, E. Thrane, H.-U. Widdel, Y.-F. Wu, and U. von Zahn, Morphology and sources of turbulence during DYANA, *J. Atmos. Terr. Phys.*, in press, 1993*a*.

Lübken, F.-J., G. Lehmacher, E. Thrane, T. Blix, U.-P. Hoppe, J. Cho, and W. Swartz, First in situ observations of neutral and plasma density fluctuations within a PMSE layer, *Geophys. Res. Lett.*, in press, 1993*b*.

Manson, A. H., C. E. Meek, and J. B. Gregory, Gravity waves of short period (5–90 min), in the lower thermosphere at 52°N (Saskatoon, Canada), *J. Atmos. Terr. Phys.*, *42*, 103–113, 1980.

Manson, A. H., C. E. Meek, and J. B. Gregory, Gravity waves of short period (5–90 min), in the lower thermosphere at 52°N (Saskatoon, Canada); 1978/1979, *J. Atmos. Terr. Phys.*, *43*, 35–44, 1981.

McIntyre, M. E., On dynamics and transport near the polar mesopause in summer, *J. Geophys. Res.*, *94*, 14,617–14,628, 1989.

Mlynczak, M. G., and S. Solomon, Middle atmosphere heating by exothermic chemical reactions involving odd-hydrogen species, *Geophys. Res. Lett.*, *18*, 37–40, 1991*a*.

Mlynczak, M. G., and S. Solomon, On the efficiency of solar heating in the middle atmosphere, *Geophys. Res. Lett.*, *18*, 1201–1204, 1991*b*.

Neuber, R., P. von der Gathen, and U. von Zahn, Altitude and temperature of the mesopause at 69°N latitude in winter, *J. Geophys. Res.*, *93*, 11,093–11,101, 1988.

Nicolet, M., The dissociation of oxygen in the high atmosphere, *J. Geophys. Res.*, *59*, 15–45, 1954.

Novikov, E. A., The energy spectrum of incompressible turbulent flow, *Dokl. Akad. Nauk SSSR*, *139*, 331–334, 1961.

Offermann, D., DYANA project survey, in *Proceedings of the 10th ESA Symposium on European Rocket and Balloon Programmes and Related Research, Cannes-Mandelieu, France, Eur. Space Agency Spec. Publ. ESA SP-317*, 369–386, 1991.

Schmidlin, F. J., The inflatable sphere: A technique for the accurate measurement of middle atmosphere temperatures, *J. Geophys. Res.*, *96*, 22,673–22,682, 1991.

Sharma, R. D., and P. P. Wintersteiner, Role of carbon dioxide in cooling planetary thermospheres, *Geophys. Res. Lett.*, *17*, 2201–2204, 1990.

Shved, G. M., L. E. Khvorostovskaya, I. Y. Potekhin, A. Demyanikov, A. A. Kutepov, and V. I. Fomichev, Measurement of the quenching rate constant for collisions CO_2 (01^10)-O: The importance of the rate constant magnitude for the thermal regime and radiation of the lower thermosphere, *Atmos. Ocean. Phys.*, *27*, 295–299, 1991.

Strobel, D. F., Parameterization of the atmospheric heating rate from 15 to 120 km due to O_2 and O_3 absorption of solar radiation, *J. Geophys. Res.*, *83*, 6225–6230, 1978.

Tatarskii, V. I., *The Effects of the Turbulent Atmosphere on Wave Propagation*, Israel Program for Scientific Translations, Jerusalem, 1971.

Thrane, E. V., and B. Grandal, Observations of fine scale structure in the mesosphere and lower thermosphere, *J. Atmos. Terr. Phys.*, *43*, 179–189, 1981.

Thrane, E. V., O. Andreassen, T. Blix, B. Grandal, A. Brekke, C. R. Philbrick, F. J. Schmidlin, H.-U. Widdel, U. von Zahn, and F.-J. Lübken, Neutral air turbulence in the upper atmosphere observed during the energy budget campaign, *J. Atmos. Terr. Phys.*, *47*, 243–264, 1985.

von Zahn, U., F.-J. Lübken, and C. Pütz, "BUGATTI" experiments: Mass spectrometric studies of lower thermosphere eddy mixing and turbulence, *J. Geophys. Res.*, *95*, 7443–7465, 1990.

Watkins, B. J., C. R. Philbrick, and B. B. Balsley, Turbulence energy dissipation rates and inner scale sizes from rocket and radar data, *J. Geophys. Res.*, *93*, 7009–7014, 1988.

Wehrbein, W. M., and C. B. Leovy, An accurate radiative heating and cooling algorithm for use in a dynamical model of the middle atmosphere, *J. Atmos. Sci.*, *39*, 1532–1544, 1982.

Weinstock, J., On the theory of turbulence in the buoyancy subrange of stably stratified flows, *J. Atmos. Sci.*, *35*, 634–649, 1978*a*.

Weinstock, J., Vertical turbulent diffusion in a stably stratified fluid, *J. Atmos. Sci.*, *35*, 1022–1027, 1978*b*.

Weinstock, J., Energy dissipation rates of turbulence in the stable free atmosphere, *J. Atmos. Sci.*, *38*, 880–883, 1981.

Widdel, H. U., Vertical movements in the middle atmosphere derived from foil cloud experiments, *J. Atmos. Terr. Phys.*, *49*, 723–742, 1987.

Wu, Y.-F., and H.-U. Widdel, Turbulent energy dissipation rates and eddy diffusion coefficients derived from foil cloud measurements, *J. Atmos. Terr. Phys.*, *51*, 497–506, 1989.

Zimmerman, S. P., and T. J. Keneshea, Turbulent heating and transfer in the stratosphere and mesosphere, *J. Atmos. Terr. Phys.*, *48*, 491–507, 1986.

Zimmerman, S. P., and E. A. Murphy, in *Stratospheric and mesospheric turbulence*, edited by B. Grandal and J. A. Holtet, pp. 35–47, D. Reidel, Norwell, Mass., 1977.

W. Hillert, G. Lehmacher, F.-J. Lübken, and U. von Zahn, Physikalisches Institut, Universitat Bonn, Nussallee 12, 53115 Bonn, Germany.

(Received March 19, 1993;
revised July 19, 1993;
accepted July 19, 1993.)